TRANSFORMING WOOD INTO A HIGH-PERFORMANCE ENGINEERING MATERIAL VIA CELLULOSE NANOCRYSTAL IMPREGNATION

by

Ashton Oriel Chan

A thesis submitted in partial fulfillment
of the requirements for the degree

of

Master of Science

in

Mechanical Engineering

MONTANA STATE UNIVERSITY

Bozeman, Montana

July 2023

ACKNOWLEDGEMENTS

I want to thank the USDA-NIFA (Grant 13058620) for funding this research project; without your investment, this research would not be possible. I would also like to especially thank my advisor Dr. Dilpreet Bajwa. He granted me this fantastic opportunity to continue my education while exploring materials science. His guidance and flexibility allowed me to expand my knowledge to areas I had never imagined when I started. He has helped me push my boundaries and become a better researcher and person. I would also like to thank my committee members: Dr. Lewis Cox, Dr. Sreekala Bajwa, and Dr. Kerry Hartman, for their time and direction on this project.

I want to acknowledge all my fellow graduate students who have helped me during my time at MSU. Specifically, I would like to thank Kenna Brown and Dr. Saptaparni Chanda for all their help in improving the technical aspects of my writing. I would also like to thank Andrew Durado and Dalton Nold for their support and patience as I learned the basics of the lab and MSU. Additionally, I would like to acknowledge Dr. Dan Samborsky and Dr. Glenn Foster for allowing me to use their resources and brainstorm machine design ideas.

TABLE OF CONTENTS

TABLE OF CONTENTS CONTINUED

LIST OF TABLES

Table Page

LIST OF TABLES CONTINUED

Table Page

LIST OF FIGURES

Figure Page

LIST OF FIGURES CONTINUED

Figure Page

NOMENCLATURE

AA = Acetic Acid

AFM = Atomic Force Microscopy

ANOVA = Analysis of Variance

Ar = Argon

ASTM - American Society for Testing and Materials

BA = Benzoic Acid

CH_4 = Methane

CI = Confidence Interval

CL = Control

CNC = Cellulose Nanocrystals

CV = Coefficient of Variation

FE-SEM = Field Emission Scanning Electron Microscopy

GPa = Gigapascals

in = Inches

kN = Kilonewton

LSD – Least Significant Difference

MOE = Modulus of Elasticity

MOR = Modulus of Rupture

MTS = Materials Testing Systems

mm = Millimeters

min = Minute

NOMENCLATURE CONTINUED

MPa = Megapascals

μm = Micrometers

N = Number of Samples

NaOH = Sodium Hydroxide

nm = Nanometers

PLA = Polylactic Acid

PHB = Polyhydroxybutyrate

PVA = Poly (vinyl alcohol)

SD = Standard Deviation

SEM = Scanning Electron Microscopy

SYP = Southern Yellow Pine Wood

ABSTRACT

A significant challenge in this world today is innovating sustainably sourced materials for advanced engineering applications. Cellulose nanocrystals (CNCs) have excellent potential in these advanced applications as reinforcement in softwood because of their inherent biodegradability, universal accessibility, and exceptional mechanical properties. This research aimed to design a novel method to impregnate cellulose nanocrystals into marginal-quality softwood to enhance its mechanical properties for advanced engineering and architectural applications. In this research, southern yellow pine (SYP) wood underwent sodium hydroxide treatment to remove lignin from the wood cells. Then, SYP samples were submerged into a surface-functionalized (by either acetic acid or benzoic acid) CNC solution and subjected to ultrasonication treatment to penetrate functionalized-CNC into the SYP. A vacuum pressure treatment for air pocket removal and functionalized-CNC impregnation followed this. After treatment, the wood was dried and underwent mechanical testing following ASTM D1037 and ASTM D2339 standards. Delignified and functionalized-CNC impregnated SYP increased the modulus of rupture (MOR) by 68% and the modulus of elasticity (MOE) by 72%. Localized MOE maps were also generated under an atomic force microscope (AFM) to characterize the material. It was found that the areas with a CNC presence have a significantly greater elasticity modulus (<20 GPa) compared to the rest of the region consisting of SYP (3.00 - 8.55 GPa) using the Hertzian Contact model. The results support a novel methodology to improve the mechanical properties of wood delignification and functionalized CNC impregnation.

1 INTRODUCTION

1.1 Motivation

Wood is a renewable material with a wide range of applications and properties. However, the rise of mass production techniques and the increasing demand for wood as a construction material has led to shortages in the availability of high-strength wood and the depletion of natural forests (Nepal et al., 2021). The lack of high-strength wood availability has resulted in a major challenge in the construction industry today: the shortage of trees aged for harvest, resulting in builders resorting to the use of alternative and more expensive building materials (Ameh et al., 2019) such as concrete or plastic polymers which are not biodegradable (Brandner et al., 2016). To meet the demand for higher-strength wood products, varieties of softwood not traditionally used in applications such as heavy construction can be treated in several ways to obtain desirable engineering properties.

The most common method to make wood suitable for advanced engineering applications is lamination, a technique/process of manufacturing wood in multiple layers such that the composite wood achieves improved strength, stability, sound insulation, appearance, or other desirable properties from the different material(s). Previous work includes laminating wood using adhesives or fasteners to bind small strips of wood together (Sotayo et al., 2020). The advantages of this technique are increased tensile strength (parallel to grain: 226 MPa to 236 MPa; perpendicular to grain: 3.17 MPa to 3.79) and compressive strength (parallel to grain: 49 to 62 MPa; perpendicular to grain: 24 to 44 MPa) according to a previous study (Manik et al., 2019).

However, disadvantages include decreased stiffness over time (Guan et al., 2010) and dimensional instability after repeated cycles (Sotayo et al., 2020).

Another common method for wood modification is delignification and densification. Delignification is a process that removes the lignin within the wood, a key structural material in the wood. However, due to its recalcitrant, heterogeneous, and complicated structure, its removal can ease modification techniques via the increase in porosity of the wood or facilitate the collapse of cell walls within the wood. Densification is the process by which wood density is increased via wood compression (Frey et al., 2018). Densification enhances the mechanical properties of wood by achieving a higher homogeneity while preserving structural directionality (Kollmann et al., 2012). However, the disadvantage of densification is the collapse of cell walls and the formation of microcracks (Frey et al., 2018). Delignification improves densification by extracting lignin from wood to disintegrate it into fibrous components, reducing the cell wall's transverse rigidity and facilitating cell wall collapse during densification (Kollmann et al., 2012). Previous studies have researched delignified and densified wood derived from fast-growing woods such as poplar in bulk form (Frey et al., 2018) and green wood form (Wang et al., 2021). These studies have found improved dimensional stability from 12% to 0% in green wood form (Wang et al., 2021) and enhanced elastic moduli from 15 GPa to 35 GPa in bulk form (Frey et al., 2018).

Wood can also be modified through impregnation. Impregnation is conducted in numerous ways, with the most common methods being full-cell and empty-cell treatments (Laks et al., 2008). The full cell method, or the Bethel method, induces an initial vacuum to remove air pockets in the wood and the cylinder. The vacuum is followed by a pressure treatment of the wood to fill the full wood cell with a desired chemical until desired chemical retention is obtained. This process yields

maximum chemical retention (Laks et al., 2008). The half-cell or the modified full-cell technique is used for water-based chemicals, which uses the same process as the full-cell technique, but with a reduced initial vacuum level (Lou et al., 2018). The empty-cell method, namely the Lowry process, uses compressed air to drive out a portion of the preservative absorbed during the pressure period (Sandberg et al., 2017). This method obtains deep preservative penetration with low net preservative retention (Laks et al., 2008). This modification technique can also be enhanced using delignification as greater amounts of nanofiller can be inserted into the wood with increased porosity. Previous studies have shown that delignification combined with full cell impregnation on Birchwood has found delignification combined with an ionic liquid treatment led to improved mechanical performance (Tensile strength increase from 70 to 375 MPa and Shore D Hardness from 53 to 82) (Khakalo et al., 2020). Additionally, it was found that empty cell impregnation treatment using nano-aluminum-oxide poplar wood resulted in an increase in elastic moduli from 0.6 to 1.4 GPa (Taghiyari et al., 2017)

Field Emission Scanning Electron Microscopy (FE-SEM) is commonly used to characterize wood. FE-SEM is an advanced technology used to capture the microstructure image of the materials. FE-SEM provides topographical and elemental information at magnifications of 10x to 300,000x, with virtually unlimited depth of field. FE-SEM can produce clear images, with spatial resolution down to 1.5 nanometers (Wang et al., 2018). FE-SEM can be used to analyze the nanocellulose. However, the disadvantages of FE-SEM are that besides surface images and chemical composition in certain modes, no surface-level mechanical properties (Wang et al., 2021) can be assessed with this method which may pose problems with materials of similar morphologies.

To address the lack of surface mechanical property assessment from FE-SEM, atomic force microscopy (AFM) can be used. AFM is a scanning probe microscopy technique wherein a probe tip contacts the sample surface. This vertical tip motion is measured via laser beam reflection from the top surface of the probe into a photodetector. AFM produces topographical images with high x–y resolution (tens of nm) and ultrahigh z-resolution (<0.1 nm). The z-resolution is several orders of magnitude greater than resolutions achievable through diffraction-limited optical microscopy. So far, AFM has been effectively used to visualize plant cell wall layers (Zimmerman et al., 2006), their architecture, arrangement, orientation, and size (length and diameter) of cellulose microfibrils (Schoeffmann et al., 2023). Disadvantages of AFM include the need for extremely smooth samples to accurately map out the sample's topography (Zimmerman et al., 2021) and the risk of AFM cantilever tip detachment during contact with the surface or in transition, resulting in tip replacement costs (Zimmerman et al., 2021).

This research aimed to develop a method to transform SYP softwood into a material suitable for advanced engineering applications, comparable to that of hardwoods (American Beech, Sugar Maple, and Live Oak), as SYP has considerably lower properties than the species described in Table 1.

Table 1: Mechanical Properties of some Wood Species (Ross et al., 2021)

Wood Species	MOE (MPa)	MOR (N)	Density (kg/m3)	Hardness(N)
American Beech	11900	103	640	5800
Sugar Maple	12600	109	640	6400
Live Oak	13700	127	880	12920
SYP(Commercial)[a]	11400	102	476.5	2814

[a] = data obtained from testing

The novelty of this research is that it combines the techniques of delignification and densification with the impregnation of a bio-based nanofiller to produce a sustainably sourced

wood product that can achieve superior mechanical properties. Various tests meeting ASTM standards, FE-SEM, and AFM were used to prove the achievement of superior mechanical properties and visualize changes in the material. In this study, southern yellow pine wood (SYP) was delignified, densified, and impregnated with functionalized cellulose nanocrystals (CNCs) as a nanofiller.

CNCs are nanomaterial derived from plants via acid hydrolysis to separate the crystalline and amorphous domains of cellulose by converting the amorphous domains into sugars or other small molecules. In contrast, the crystalline regions become rigid nanoparticles that are 80-100 nm in length (Le Gars et al., 2019). CNCs were used as a nanofiller due to their great abundance as they are sourced from plant material (Chanda et al. 2021), high crystallinity (54–88%), excellent mechanical properties (tensile strength 7 GPa, elastic modulus of 150 GPa), lightweight, transparency, relatively low cost, and their versatile surface modification properties (Wang et al., 2021). As a result of the surface modification properties, these CNCs can be further strengthened via the Fischer–Speier esterification, using benzoic acid (BA) or acetic acid (AA) and blending it into the CNC (Tang et al., 2013 and Shojaeiarani et al., 2018). BA and AA modify the surface of CNC by introducing functional groups onto the surface, allowing for the conversion of surface hydroxyls into esters via Fisher esterification (Rana et al., 2021), resulting in rough and irregular surfaces to encourage ductile fracture of the material resulting in enhanced mechanical properties when blended into polymers such as PLA (Young’s modulus increase from 3.33 to 4.23 GPa) (Shojaeiarani et al., 2018). Additionally, the surface acetylation of CNC via the reaction between the acetic anhydride and hydroxyl groups on the surface of the CNC is hypothesized to enhance the dispersion of CNC and improve mechanical performance (Lin et al., 2011). It is hypothesized

that the insertion of this high-engineering performance functionalized CNC into the wood will transform softwood (SYP) into a high-performance engineering material.

1.2 Objectives

This research aimed to design a novel method to impregnate cellulose nanocrystals into marginal-quality softwood to enhance its mechanical properties for advanced engineering and architectural applications. The following three objectives were developed to achieve this aim:

The first objective was to optimize and validate an effective process of impregnating wood with functionalized CNCs and determine critical variables influencing CNC impregnation into the wood. A potential treatment hypothesized to influence CNC impregnation was a solution-based alkali delignification technique, as delignification would increase the porosity of wood to enhance CNC impregnation. Delignification was followed by an ultrasonication technique where an aqueous solution of functionalized CNC will be introduced into a chamber for even nanodispersion and impregnation into the wood. It was hypothesized that the ultrasonication would impregnate the wood with CNCs while evenly dispersing the CNC nanodispersion. The samples were then transferred into another vessel for vacuum pressure impregnation to remove the air pockets and impregnate additional CNC into the porous structure of the wood.

The second objective was to investigate the microstructural, physiological, and compositional changes in wood impregnated with CNC. Localized surface properties were examined using atomic force microscopy, while microstructural and morphological changes in the modified wood were analyzed using field emission scanning electron microscopy.

The third objective was to evaluate the physical and mechanical properties of CNC-impregnated wood. The treated samples were conditioned and tested for their moisture resistance, dimensional stability, internal bond, hardness, fastener strength, flexural strength, and tensile strength properties using the ASTM D1037 standard. Moisture resistance was measured using the linear expansion test. The dimensional stability of impregnated wood samples was evaluated using moisture absorption and thickness swelling. Internal bond was measured using the lap shear test. Hardness was measured using the Janka ball hardness test. Fastener strength was tested using nail and screw withdrawal tests. Flexural properties were measured using the flexural test.

2 LITERATURE REVIEW

2.1 Modification of Wood and Cellulose Nanocrystals

Since the dawn of civilization, timber has been used as a structural material due to its ubiquity and low cost. However, depending on the species, wood comes with a vast array of properties. Hardwoods have a high stiffness and high tensile strength yet grow slowly. Softwoods such as southern yellow pine are porous, resulting in a low MOE and MOR while growing quickly. Due to a lack of material properties, wood is typically modified in various ways to obtain the desired properties. Its susceptibility to moisture and its orthotropic microstructure makes traditional timber undesirable for macrostructural applications alone (Brandner et al. 2016). As a result, wood is modified through several methods to make the material suitable for such applications. A promising method is impregnating wood with a highly tunable and high-strength material known as CNC (Habibi et al., 2014). This review aims to discuss the various methods utilized to modify wood and CNC and their advantages and drawbacks in producing a high-performance engineering material.

2.1.1 Laminated Timber

A common method to make wood suitable for advanced engineering material applications is through laminated timber, a technique/process of manufacturing wood in multiple layers, such that the composite wood achieves improved strength, stability, sound insulation, appearance, or other desirable properties from the different material(s). An example includes laminating wood using an adhesive to bind small strips of wood together (Sotayo et al., 2020). The advantages of this technique are increased tensile strength (parallel to grain: 226 MPa to 236 MPa perpendicular

to grain: 3.17 MPa to 3.79 (Manik et al., 2019) and compressive strength (parallel to grain: 49 to 62 MPa, perpendicular to grain: 24 to 44 MPa (Manik et al., 2019) However, disadvantages include a decrease in stiffness over time and dimensional instability (Balasbaneh et al., 2020). Laminated wood is commonly arranged into two patterns: CLT or GLT. GLT consists of timber-glued layers in the same grain-facing direction, while CLT alternates each grain-facing layer by 90°. The advantages of GLT are increased tensile strength parallel to the grain, making it advantageous for structural applications, while CLT provides increased strength parallel and perpendicular to the grain, at the drawback of increased costs (Brandner et al., 2016). As a result of these wood strengthening techniques, CLT and GLT allow for larger-scale applications of smaller wood samples.

2.1.2 Delignification and Densification

In natural wood, lignin is an important filler and adhesive that bonds to hemicelluloses and fibers owing to its abundant functional groups and amorphous network structure. The chemical removal of lignin in wood can alter its structure and chemical composition, as a powerful engineering material process. Delignification leads to more exposure of cellulose fibrils, which are originally embedded in the lignin and hemicellulose matrixes. Additionally, the delignified wood maintains the anisotropic, hierarchically porous structure of natural wood but with more nanopores within the cell walls (Li et al., 2018). This increased porosity facilitates the collapse of cell walls under high pressures (Qian et al., 2019).

There are various delignification methods, the most common being a heated alkali solution treatment (Zhu et al., 2016). In a 2019 paper by Qian et al., Douglas fir sawdust samples were submerged within a heated sodium hydroxide solution at different times and temperatures. The

solid residue was removed and washed twice with vacuum filtration to maximize lignin extraction. Another 2022 paper by Kuai et al. used a similar technique, delignifying poplar wood with and impregnating it with sodium silicate because it is an environmentally friendly, flame retardant, and low-cost inorganic modifier. This treatment facilitated increases in MOE, MOR, and compressive strength by 5, 2.4, and 27.2 times, respectively, when combined with densification. However, this treatment's drawbacks are that the delignified wood was damaged or broken into pieces in the bleaching solutions, resulting in diminished mechanical properties (Li et al., 2019). As a result, another common method to delignify wood is through steaming (Li et al., 2019). In this paper, basswood was steamed in hydrogen peroxide, which resulted in a 97% extraction in lignin while retaining over 90% cellulose. However, the drawback of this method is the presence of microcracks in the wood sample, thus making the wood susceptible to crack propagation.

From delignification, other combined wood treatments allow changes regarding desired engineering properties to be easily achieved (Spear et al., 2021). Many of these combined modification methods achieve stunning additional functionality in the wood, e.g., tensile strength, compressive strength (Wang et al., 2018), photoluminescence, electrical conductivity, sensors, transparency, etc. (Spear et al., 2021). However, this comes at the cost of the original material properties that the lignin provides (Karimi et al., 2006).

Heat treatment is a common method to add to delignification and densification (Song et al., 2018). This treatment is a heat pre-treatment prior to delignification and densification. This method effectively reduced the thickness of the wood by 80%. Additionally, a more than tenfold increase in strength, toughness, and ballistic resistance was observed. Those increases in mechanical properties, compared to past studies, were a massive improvement to prior research

where only the heat treatment was used, which led to increased resistance to rot (Esteves et al., 2009) but a 50% decrease in hemicellulose content, which leads to a similar decrease in bending strength. The decrease likely occurred due to a lack of total collapse within the cell walls, which was solved by Song et al. by adding delignification.

2.1.3 Wood Impregnation

Impregnation is a process in which chemical substances are introduced into the wood to improve its characteristics and impart new properties; the process allows the wood to obtain desirable properties from the filler material while retaining its original form. Common ways to impregnate wood include the full-cell, half-cell, and empty-cell treatments. The full-cell method induces an initial vacuum to remove air pockets in the wood and the cylinder, followed by a pressure treatment of the wood to fill the full wood cell with a desired chemical until desired chemical retention is obtained. This process yields maximum chemical retention (Laks et al., 2008). For water-based chemicals, the half-cell, or the modified full-cell technique, is used, which uses the same process as the full-cell technique, but with a reduced initial vacuum level (Walker et al., 2006). This is commonly done for water-based preservatives and yields lower solution uptake. The empty-cell method uses compressed air to drive out a portion of the preservative absorbed during the pressure period (Sandberg et al., 2017). This method obtains deep preservative penetration with a low net preservative retention level (Laks et al., 2008). This modification technique can also be enhanced using delignification, as with increased porosity, increased amounts of nanofiller can be inserted into the wood. Previous studies have shown that delignification combined with full cell impregnation on Birchwood has found delignification combined with an ionic liquid treatment led to improved mechanical performance (Tensile strength

increase from 70 to 375 MPa and Shore D Hardness from 53 to 82) (Khakalo et al., 2020). Additionally, it was found that empty-cell treated and nano-aluminum-oxide-impregnated poplar wood increased elastic moduli from 0.6 to 1.4 GPa (Taghiyari et al., 2017). Common tools used for impregnation include vacuum pumps to induce vacuum, as well as air hoses to induce air pressure (Khakalo et al., 2020). Autoclaves are also used if pressure and heat treatment are desired (Laks et al., 2008).

Common chemicals to impregnate wood include acids such as aluminum chloride to reduce the surface energy required for heat treatment (Wang et al., 2022) or various fungicides such as creosote, zinc borate of copper azole to increase the wood's resistance to rot from fungi (Laks et al., 2008). Other common chemicals, such as nano-aluminum-oxide or wood bark, are typically materials with superior mechanical properties relative to the host polymer. Advantages of this method include increased bonding strength for a wood bark nanofiller (10-60 % depending on the wood species (Widyorini et al., 2020)) and increased durability (measured in increment of resistance %) of wood (susunek) by approximately 100% (Farah et al., 2021) for nano-aluminum-oxide. However, adding inorganic metal-oxide nanofillers results in the loss of gloss, transparency, and flexibility (Marathe et al., 2008).

Nanofillers can enter wood either through solution blending or in situ. Solution blending is the addition of a polymer (and other present compounds) in a suitable solvent and applying high shear forces for dispersion (Nikolic et al. 2015). It is also possible to pre-disperse nanomaterials in a solvent and transfer this dispersion to the polymer (Nikolic et al. 2015). In-situ addition is often beneficial as smaller molecules can easily diffuse between nanoparticles and ease nanoparticle separation (Nikolic et al. 2015). This method is especially convenient for coatings, industrial

indoor lacquers for furniture, and parquets. These coatings allow high production speed, low VOC (volatile organic compound) content, and good mechanical and chemical resistance due to the high network density that can be formed (Marathe et al., 2008).

Ultrasonifiers are also common tools used for impregnation due to their high dispersing forces as they convert mechanical or electrical energy into high-frequency acoustical energy (Nikolic et al., 2015). High intensity ultrasonication waves produce a strong mechanical oscillating power through the formation, expansion, and implosion of microscopic gas bubbles when the molecules in a liquid absorb the ultrasonication energy. The breakage of aggregates is controlled by the energy input influenced by power, time, and dispersion volume. (Shams et al., 2005). However, there are some instances in which high shear forces are not adequate to disperse nanoparticles in a polymer matrix completely, and proper dispersion remains a significant hurdle for the wider use of nanoparticles; indeed, most of the nanocomposites reported still retain some level of micron-sized clusters (Schaefer et al., 2007).

2.1.4 Cellulose Nanocrystals (CNC)

A nanofiller that is used to strengthen polymers is CNC. CNC is prepared by hydrolyzing and removing the amorphous domains of cellulose using highly concentrated acids in a process called acid hydrolysis (Moon et al., 2011). The dimensions and crystallinity of the CNC depend on the conditions of extraction and the source of cellulose, with crystallinity increasing alongside the cellulosic purity of the material (Moon et al., 2011). During acid hydrolysis, the nature of the acid used is extremely important because it affects the dispersion property. For example, if hydrochloric or hydrobromic acid is used, the dispersion is extremely limited, resulting in the aqueous suspensions tending to flocculate. However, in the case of sulfuric and phosphoric acids,

the hydroxyl groups of cellulose surface yield sulfate or phosphate esters, which improve the dispersion of CNC in water (Habibi et al., 2010).

CNCs have been used over the past two decades to strengthen natural and synthetic polymers (Younas et al., 2019). Examples include gelatin hydrogels reinforced by CNC (Ooi et al., 2016), PVA-CNC as a tissue engineering scaffold, and natural rubber-CNC (Neto et al., 2016), and CNC-reinforced PLA (Shojaeiarani et al., 2018) to name a few. That is because CNCs are a high-strength material with a tensile strength of 7 GPa, elastic moduli of 150 GPa, and a high crystallinity of 54–88% (Habibi et al., 2014). CNCs also have tunable surface chemistry, allowing for the introduction of surface charges and functional groups onto the surface of the CNC to confer new engineering properties (Moon et al., 2011). These properties allow CNCs to be used as reinforcement to develop sustainable, flexible, and superior-performance engineering materials. However, a major drawback of CNCs is their hydrophilic nature, which hinders their direct dispersion in nonpolar hydrophobic polymeric matrixes (Paskdel et al., 2021). On the other hand, this effect can be mitigated using surface functionalization (Mekonnen et al., 2021).

2.1.5 Surface Functionalization of Cellulose Nanocrystals.

CNC has a strong potential as a surface-functionalized nanofiller due to its vast abundance of -OH groups (Lamouroux et al., 2016). A common technique used to functionalize CNCs is chemical-aided esterification due to its simplicity (Lamouroux et al., 2016). Esterification is a chemical reaction in which two reactants (typically an alcohol and an acid) form an ester as the reaction product. With CNC, the −OH groups serve as the alcohol, and an acid, such as acetic acid (Tang et al., 2013) or benzoic acid (Shojaeiarani et al., 2018), serves as

the second reactant. With these reagents, the mechanical properties such as crystallinity (from 64% to 80-83%) with acetic acid (Tang et al., 2013) and Young's modulus by 20% with benzoic acid (Shojaeiarani et al., 2018) of CNC are enhanced. The main drawbacks of the chemical-aided dispersion techniques are the use of toxic and sometimes expensive chemicals, longer reaction time, critical control of reaction conditions, and disposal of chemicals (Chanda et al., 2021).

Another method to functionalize CNC is through polymer grafting. This method is incredibly attractive due to the large-scale availability and variety of functional polymers (Zhang et al., 2021). The polymer grafting method uses functional polymer brushes to either "grafting onto" or "grafting from" the CNC. "Grafting onto" is when pre-synthesized polymer chains are attached to reactive groups onto the surface hydroxyl groups of cellulose, while the "grafting from" approach uses ring-opening polymerization to grow polymer brushes nano celluloses using the surface hydroxyl groups as initiating sites (Islam et al., 2013) A major advantage of "grafting onto" include steady control as the molecular weight of the attached characterized before grafting (Missoum et al., 2013). However, a disadvantage to the "grafting onto" approach is that high grafting densities are unattainable due to the steric hindrance of the polymer chains. "Grafting from" is the process of mixing the cellulosic nanoparticles or the activated cellulosic nanoparticles with a monomer and an initiator agent to induce monomer polymerization from the nanoparticle surface (Missoum et al., 2013). An example of this strategy being used is when Hydroxyazetidinium salts were used to surface-modify CNC to delay the thermal degradation of CNC (Forsgren et al., 2018). The study found that these salts could not improve the thermal stability of CNC due to the alkaline nature of the salt while improving the elastic modulus by a

factor of three. However, the suggested drawback of using this salt is the alkaline nature of the dispersions resulting in the degrafting of functional groups (Forsgren et al., 2018).

Another polymer grafting strategy used is the “grafting from” strategy. This strategy has proven to be a remarkably effective way to create high grafting densities on the surface due to the lower viscosity of the medium and the limitation of steric hindrance (Littunen et al., 2011). However, a major drawback to this approach is that it is difficult to control and determine the precise molecular weight of the grafted polymer, which is usually limited to a low degree of polymerization (Littunen et al., 2011). An example is in a 2008 paper by Habibi et al., which used this approach to create PCL-grafted ramie CNC, which resulted in a 110% increase in Young’s modulus compared to when the CNC was not grafted (Habibi et al., 2008).

Silanization can also functionalize CNC by using a silane to graft onto the CNC. Silane functionalization of CNC is an attractive process due to silane’s: large-scale availability, cost-effectiveness, variety of functional moieties, ease of the reaction chemistry, and because it is a mild aqueous reaction medium (Mekonnen et al., 2021). An example 2021 study by Mekonnen et al., silanization was grafted onto CNC to increase corrosion resistance within polyurethane via an aqueous medium consisting of CNC and silane. The study found that silane increased the thermostability of the CNC (peak degradation at 460 ˚C rather than 312 ˚C) as well as reduced corrosion resistance and water absorption (3% for an untreated CNC polyurethane composite compared to 2% for a silanated CNC polyurethane composite). This method was also used as a polymer reinforcement for PLA (Chanda et al., 2018), which led to enhanced thermal stability (peak degradation at 310 ˚C rather than 270 ˚C) but decreased crystallinity (61.7% down to 55.1%).

A relatively newer functionalization technique is plasma-induced surface modification (Chanda et al.,2021). Plasma-induced surface modification is when a nanometric layer is deposited on the surface of nanoparticles, which then tunes the surface chemistry of the CNC (Taschuk et al., 2010). Plasma is typically dispersed through a gas reactor (Chanda et al., 2021). This treatment has applications in developing cellulose films (Bhanthumnavin et al., 2016) and sheets (Couturaud et al., 2015). Results include a study where ABS-CNC was plasma treated via an ethylene reactor, resulting in a 60% increased impact strength compared to the non-functionalized CNC (Alanis et al., 2019). Another 2020 study by Matouk et al. used various Argon-based gases in a plasma reactor to functionalize CNC films. This functionalization technique decreased the hydrophilicity of CNC and slightly increased the crystallinity of Ar/CH_4 gas (Matouk et al., 2020). The drawbacks of this treatment process are that the plasma treatment of cellulose powders or fibers is difficult due to suction, spreading, or limited contact (Matouk et al., 2020). All these functionalization techniques aid in the dispersion of CNCs in the hydrophobic polymer matrices.

3 MATERIALS AND METHODOLOGY

3.1 Materials

SYP was studied due to its low-cost, lightweight construction applications, and its limitations due to variability (Briggs et al. 2010). Commercial SYP boards (6.35 mm thickness x 35 mm width) were sourced commercially from a local wood products store. Sodium hydroxide (NaOH formula weight = 40.00 g/mol) purchased from Fisher Chemical (Fair Lawn, NJ) was used as a delignification agent. CNC with dimensions of 10–15 nm in width and 80–100 nm in length and aspect ratios of 5–10 was provided by the USDA (US Department of Agriculture) Forest Products Laboratory (Madison, WI, USA). These CNCs were extracted from softwood pulp via sulfuric acid hydrolysis and desulfated using hydrothermal treatment. Glacial AA (molecular weight 60.05 g/mol) obtained from Fisher Chemical (Fair lawn, NJ) and BA pellets (formula weight = 122.12 g/mol) obtained from Carolina Biological Supply Company (Burlington, NC) were used as grafting agents. Deionized water bought from Millipore (Burlington, MA) acted as the solvent.

3.2 Preparation of Samples

3.2.1 Specimen Preparation

Specimens of SYP were cut into strips of 6.35 mm thickness x 180 mm length x 17.50 mm width using a bandsaw, as displayed in Figure 1. All resulting dimensions were measured using a caliper and rounded to the nearest hundredth. Specimens were oriented treatment code face up, down, and sideways to measure length to ensure dimensional consistency. Thickness

and width were measured at five different points: two points were at the ends, two were 25 mm away from the ends, and one was 51 mm from the left.

Figure 1. Southern Yellow Pine Wood Specimen

Figure 2 displays the resulting sample for the hardness, screw withdrawal, and nail withdrawal tests. 4 SYP strips cut length parallel to the grain of 180 x 17.50 x 6.35 mm were prepared and treated. The strips were stacked, one atop another, adhered using Gorilla super glue, and clamped together overnight, resulting in a thickness of 25 mm. A point was marked lengthwise every 25 mm, with the third point marked with an X to indicate the left end of the sample.

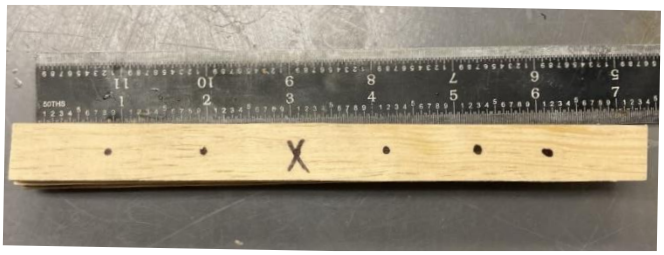

Figure 2. Southern Yellow Pine Wood Specimen for: Hardness, Screw Withdrawal, and Nail Withdrawal Tests

FE-SEM samples were prepared using a slice of wood cut perpendicular to the grain towards the center of an SYP strip sample and then cut into thin slices using a miter saw and box. These samples were polished at 4000 grit and mounted onto a commercially purchased epoxy

resin. Samples were of 5 mm thickness x 3 mm length x 3 mm width, so multiple samples could be mounted for FE-SEM imaging.

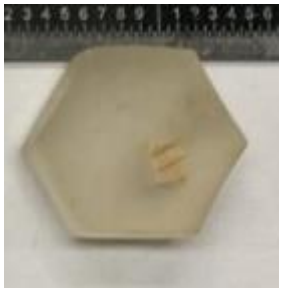

Figure 3. Southern Yellow Pine Wood Specimen for: Field Emission Scanning Electron Microscopy

AFM samples were prepared using a slice of wood cut perpendicular to the grain towards the center of an SYP strip sample and then cut into thin slices using a box cutter. The sample sizes were 0.5 mm thickness x 3 mm length x 4 mm width so that multiple samples could be mounted for analysis.

Figure 4. Southern Yellow Pine Wood Specimen for: Atomic Force Microscopy

3.2.2 Treatment Classification

To simplify the treatment and formulations used, they were recorded as abbreviations. Preceding numbers indicate a percent solute. The numbers were followed by letters representing

different treatments: CL is for control, N is for a % weight NaOH delignification treatment, CNC represents % weight CNC impregnation treatment, AA is the % volume added into a nanosuspension, and BA is the % weight added into a nanosuspension. VP is simply vacuum pressure treated, without CNC. These treatments are summarized in Table 2.

Table 2: Treatment Nomenclature

Treatment	Factor Levels and Description
CL	Control/Untreated
N	% Concentration of Sodium Hydroxide Two levels: 0 wt.%, 3 wt.%
CNC	% Concentration of cellulose nanocrystals Two levels: 0 wt.%, 1 wt.%, 2 wt.%, 5 wt.%
BA	% Concentration of benzoic acid nanosuspension Two levels: 0 wt.%, 2 wt.%
AA	% Concentration acetic acid nanosuspension Two levels: 0 vol.%, 2 vol.%
VP	Vacuum Pressure Treated (No CNC)

Formulation Example: 3N2AA2CNC – 3% NaOH, 2% acetic acid, and 2% CNC treated.

3.2.3 Nanosuspensions of Cellulose Nanocrystals

CNC nanosuspensions were developed to identify optimal surface modification agents. To create a nanofiller with highly desirable mechanical properties, surface grafting of CNCs using BA and AA was done using procedures reported in the literature (Shojaeiarani et al., 2018). BA pellets were pulverized via mortar and pestle and poured into a 300 ml solvent of DI water at 2 wt.%. BA solution was stirred at 600 rpm and melted at 140 °C for 4 hours onto a stir plate to enhance solubility throughout the solvent. BA solution was cooled for 45 minutes to prevent the melting of CNC. CNC chunks were pulverized and added to the BA. The CNCs were stirred overnight at concentrations of 1, 2, and 5 wt.%. For AA, glacial AA was poured into a 300 ml solvent of DI water at 2 vol.%. The AA was stirred at 600 rpm for 5 minutes due to its

high solubility. Chunks of CNCs were pulverized and added to the AA at 1, 2, and 5 wt.% concentrations, and stirred overnight.

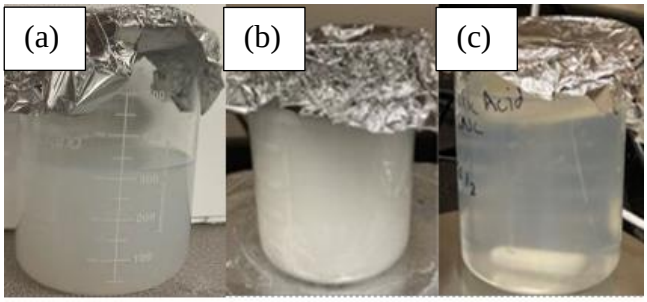

Figure 5. CNC Nanosuspensions (a) 2CNC (b) 2CNC2BA (c) 2AA2CNC

3.2.4 Delignification

Delignification was conducted using procedures as reported in the literature (Qian et al., 2019) and optimized for SYP to facilitate lignin removal and the collapse of cell walls during vacuum pressure treatment. A 300 ml, 3 wt.% sodium hydroxide (NaOH) solution was stirred at 600 rpm in a low-density polyethylene container and heated to 80 °C on a hotplate. Ten strips of SYP were immersed using glass beakers. The SYP was immersed for 2.5 hours and removed for drying (Figure 6). The wood was dried on an oven rack at 70 °C overnight prior to additional testing or treatment.

Figure 6. Delignification of Southern Yellow Pine Wood

3.2.5 Ultrasonication

Dried SYP strips were placed into a thermos and separated using a polylactic acid (PLA) disk with ten slots in Figure 7a. The (BA or AA) grafted CNC was poured into the thermos and rested for 15 minutes, as displayed in Figure 7b. In Figure 7c, the SYP strips were then ultrasonicated for 25 minutes at 18 kHz in a Hielscher UIP1000hdT ultrasonicator (Berlin, Germany) to ensure even dispersion of the CNC nanosuspension and minor impregnation throughout the SYP samples (Kargarzadeh et al., 2017). Upon ultrasonication, the samples remained in the thermos for additional treatment.

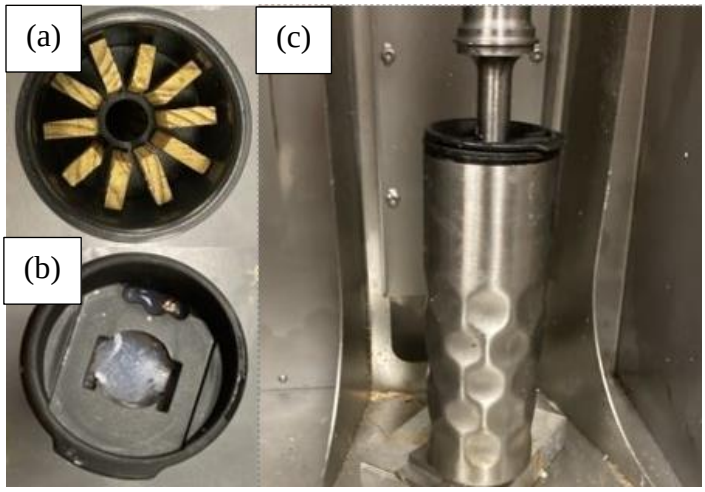

Figure 7. Ultrasonication Process: (a) Sample Loading (b) Nanosuspension Loading (c) Ultrasonicator Insertion

3.2.6 Vacuum Pressure Impregnation

Ultrasonicated SYP strips encased within a thermos were inserted into the vacuum pressure vessel shown in Figure 8. The vessel was designed to hold an 80 kPa vacuum and an 800 kPa pressure to impregnate the surface-grafted CNC solution into the samples. The vacuum was applied using a Rocker 410 vacuum pump in Figure 8a and pressurized using an 800 kPa air hose

attached to the laboratory building in Figure 8b. The vacuum pressure vessel was a 102-mm diameter steel pipe nipple and two iron caps sealed using plumbing tape.

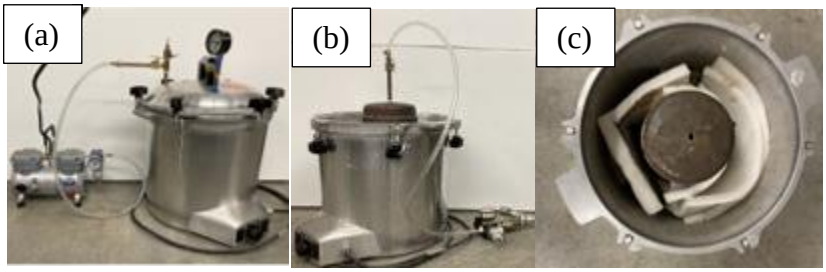

Figure 8. Vacuum Pressure Vessel Setup: (a) Vacuum Treatment Setup (b) Pressure Treatment Setup (c) Top view of Vacuum Pressure Vessel

3.3 Characterization

3.3.1 Field Emission Scanning Electron Microscopy

A method commonly used to characterize wood is FE-SEM, an advanced technology used to capture the microstructure image of the materials. FE-SEM provides topographical and elemental information at magnifications of 10x to 300,000x, with virtually unlimited depth of field. FE-SEM produces clear images with spatial resolution down to 1.5 nanometers. In this study, FE-SEM was used to analyze the cell walls of the material. However, the disadvantages of FE-SEM are that it only produces surface images (Reza et al., 2015) and chemical composition (Abraham et al., 2020) in specific modes. However, this method cannot assess surface-level mechanical properties, which may pose problems with materials containing similar morphologies, such as wood and CNC.

3.3.2 Atomic Force Microscopy

Atomic force microscopy was used to address the lack of surface mechanical property assessment on a localized scale. AFM is a scanning probe microscopy technique wherein a probe

tip is ‘rastered’ over the sample surface. This vertical tip motion is measured via laser beam reflection from the top surface of the probe into a photodetector. AFM produces topographical images with high x–y resolution (tens of nm) and ultrahigh z-resolution (<0.1 nm). The z-resolution is several orders of magnitude greater than resolutions achievable through diffraction-limited optical microscopy. So far, AFM has been effectively used to visualize plant cell wall layers (i.e., their architecture, arrangement, orientation, and the size of their cellulose microfibrils) (Zimmerman et al., 2006). Disadvantages of AFM include the need for extremely smooth samples to accurately map out the sample's topography and the fragility of the AFM cantilever tips, resulting in tip replacement costs.

This study used AFM to provide details of SYP topography and detect CNCs within a localized area (1 µm x 1µm) and of a CNC-treated SYP sample through various methods. A Cypher S (asylum research) AFM was used with Bruker RTESPA-525 probes (spring constant: 200 N/m, resonance frequency: 525 kHz). Surface topography was mapped using tapping mode, where the AFM cantilever oscillates at or close to its resonance frequency near the sample's surface. Modulus maps were collected using the fast force mapping mode of the instrument, which rapidly collects ~300 force-displacement curves per second as the probe rasters back and forth across the desired sampling area. To extract a material modulus value from each force-displacement curve, each pixel was fit with a Hertzian contact mechanics model. The Hertzian contact mechanics model simulates a sphere rolling onto a flat surface, as shown in equation 1. Modulus maps of 1 μm^2 with a pixel size of 256 allowed a pixel resolution of 3.9 nm (1 µm ÷ 256 = 0.0039 µm, or 3.9 nm). Modulus maps were generated using the Hertzian contact model,

assuming a sphere is rolling onto a flat surface. The calculation for the Hertzian contact model is as follows:

$$F = \frac{2Etan(\alpha)}{\pi(1-\nu^2)\delta^2} \quad \text{(Equation 1)}$$

The Hertzian model gives the force F as a function of the indentation (δ), Young's modulus (E), α is the tip opening angle (35°), and ν the Poisson ratio (arbitrarily assumed to be 0.5).

3.3.3 Fourier-Transform Infrared Spectroscopy (FTIR)

Fourier-transform infrared spectroscopy (FTIR) is a technique used to obtain an infrared spectrum of absorption or emission of a solid, liquid, or gas. In this study, FTIR was used to analyze the chemical composition of the SYP impregnated with functionalized-CNC using a Thermo-Scientific FTIR/ATR spectrometer, model Nicolet iS50 (ThermoFisher Scientific, Madison, WI). The motivation for using FTIR is to determine and compare the chemical composition of f-CNC treated and untreated SYP and see the resulting chemical changes in the functional groups due to hydrogen bonding resulting from CNC and f-CNC when impregnated into wood. The spectra resulted from 32 times averaged scans at five different points across the sample and were acquired at a resolution of 4 cm^{-1} from 400 to 4000 cm^{-1}.

3.4 Design of Experiment

All treatments consisted of combinations of individual treatments described in Table 2. Due to the multi-step treatment process full factorial design was implemented for the treatment of SYP to test four-factor effects: the effect of delignification, the effect of CNC impregnation at different concentrations, the effect of BA functionalization of CNC, and the effect of AA

functionalization of CNC. The experimental design started with 32 different flexural test treatments, as shown in Table 3, using a modified full factorial design test. The flexural test determining MOR and MOE are strong indicators of engineering performance in a sample. Due to the redundancies in the treatment combinations that went beyond the scope of this experiment, that number of treatments was reduced to a net total of 24 treatments for the flexural test. Concentrations were limited for certain treatments, such as acid suspension and delignification treatment, as they were used to understand the effect of each treatment, such as delignification and AA/BA surface functionalization of CNCs. Upon testing these treatments, the top 6 treatments obtained from the MOR and MOE results were selected for further physical and mechanical properties testing described in Section 3.5.5.

Table 3: Treatment Summary with Linear Combination Factors

Treatment	Factor Levels
Sodium Hydroxide (N)	0,3
Cellulose Nanocrystals (CNC)	0,1,2,5
Acetic Acid (AA)	0,2
Benzoic Acid (BA)	0,2
Unique Formulation Total	2 x 4 x 2 x 2 = 32
Combined BA/AA Removal	8
Unique Formulation Net Total:	2 x 4 x 2 x 2 – 8 = 24

3.5 Physical and Mechanical Properties Tests

3.5.1 Density

To evaluate the impregnation rate of SYP via CNCs, the relative change in density ($\Delta\rho$) was measured as displayed in Equation 2. This test aims to determine the effects of vacuum pressure treatment CNC impregnation on the density of the material; thus, a gain of density

comparison was conducted before and after vacuum-pressure treatment. Five 6.35 mm thick x 180 mm length x 17.5 mm width strips pre-vacuum pressure treated (i.e., delignified or untreated) strips were dried at 70 ˚C for 24 hours and weighed and measured. Density was then measured following the treatment. The samples were then vacuum pressure treated. The resulting samples were at 70 ˚C for 24 hours and weighed. The calculation for the change in density was calculated as follows:

$$\Delta\rho = \frac{\rho_t - \rho_0}{\rho_t} * 100\% \qquad \text{(Equation 2)}$$

where $\Delta\rho$ is there percent change in density, ρ_0 is the density of the wood before treatment, and ρ_t is the density of the SYP after treatment.

3.5.2 Water Absorption Test

To determine the liquid absorptiveness and resilience properties of SYP, water absorption tests were conducted. ASTM D1037 standards were followed accordingly for the fixture and calculations (American Society for Tests and Materials, 2018). Five SYP strips of 6.35 mm thickness x 180 mm length x 17.50 mm width were prepared and treated. The mass of each wood strip was measured. Then, the wood strips were submerged in 25 mm of water for 24 hours in a polypropylene container. Samples were held down with aluminum wire and glass beakers, as shown in Figure 9a. The samples were left to dry for 10 minutes, and their resulting masses were measured in Figure 9b. The moisture absorption was calculated in the following equation:

$$\text{WA}\,\% \;=\; 100 \cdot \frac{m_w - m_d}{m_d} \qquad \text{(Equation 3)}$$

Here WA% is the water absorption, m_w is the mass of the sample when wet, and m_d is the mass of the sample when dry.

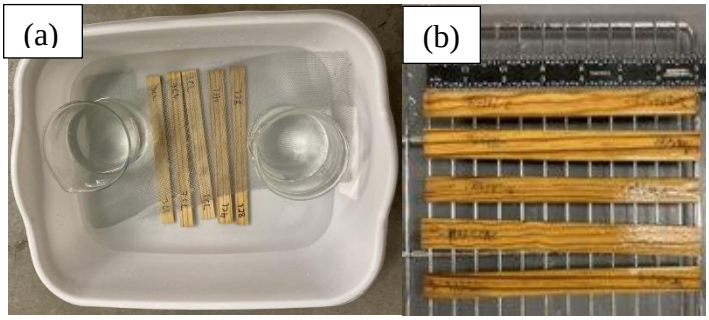

Figure 9. Thickness Swelling and Water Absorption Test Setup (a) Soaking (b) Drying

3.5.3 Thickness Swelling Test

To measure the hygroscopic properties of SYP, thickness swelling tests were conducted. ASTM D1037 standards were followed accordingly for the fixture and calculations (American Society for Tests and Materials, 2018). The same strips and submersion procedure were used from section 3.5.2, with the only difference being the thickness measurement aspect before and after submersion. The moisture absorption was calculated using the following equation:

$$T_s\,\% \;=\; 100 \cdot \frac{t_w - t_d}{t_d} \qquad \text{(Equation 4)}$$

where T_s % stands for the thickness percentage difference of the sample, t_w represents the thickness of the sample after being submerged for 24 hours and dried for 10 minutes, and t_d represents the initial thickness of the sample when dry.

3.5.4 Linear Expansion Test

Linear expansion tests were conducted to measure SYP's dimensional stability in atmospheric humidity. ASTM D1037 standards were followed accordingly for the fixture and calculations (American Society for Tests and Materials, 2018). Five 6.35 mm thick x 180 mm length x 17.50 mm width strips of SYP were prepared and treated. These samples were inserted into an ESPEC EPL-4H Temperature Humidity Chamber (Hudsonville, MI). In Figure 10, the

samples were placed onto a 4-tier oven rack and spread out with at least 6 mm space between each sample. The length of each wood strip was measured at 50% humidity at 20 °C for 24 hours and then at 90% humidity for 24 hours, and their lengths were compared. The percentage difference was calculated using the following equation:

$$L_e = 100 \cdot \frac{L_{90} - L_{50}}{L_{90}} \qquad \text{(Equation 5)}$$

where L_e is linear expansion, L_{90} is the mass of the SYP sample at 90% humidity, and L_{50} is the mass of the SYP sample at 50% humidity.

Figure 10. Linear Expansion Test Setup

3.5.5 Flexural Test

Flexural tests were conducted to determine the strength and stiffness of SYP samples. ASTM D1037 standards were followed accordingly for fixtures and calculations (American Society for Tests and Materials, 2018). For each treatment, ten 6.35 mm thickness, 180 mm length, and 17.5 mm width strips were randomly selected from a stockpile of samples and treated to minimize variation. The SYP was placed onto an adjustable span with rollers (gap distance: 127 mm) until the center length of the sample met the anvil. A Mark-10 universal testing machine (Copiague, NY) with a 500 N load cell applied a downward force at a 3 mm/min rate until the samples

fractured, as shown in Figure 11. The fractured sample is displayed in Figure 12. After testing, MOE and MOR were calculated using the following equations:

$$E = \frac{L^3 \Delta P}{4bd^3 \Delta y} \quad \text{(Equation 6a)}$$

$$R = \frac{3PL}{2bd^2} \quad \text{(Equation 6b)}$$

where E represents the modulus of elasticity, R represents the modulus of Rupture, L represents the length of the sample, P represents the peak load of the load-deflection curve, ΔP/Δy is the slope of the straight-line portion of the linear regression load-deflection curve at 30 % of the peak load, b is the breadth/width of the sample, and d is the depth/thickness of the sample.

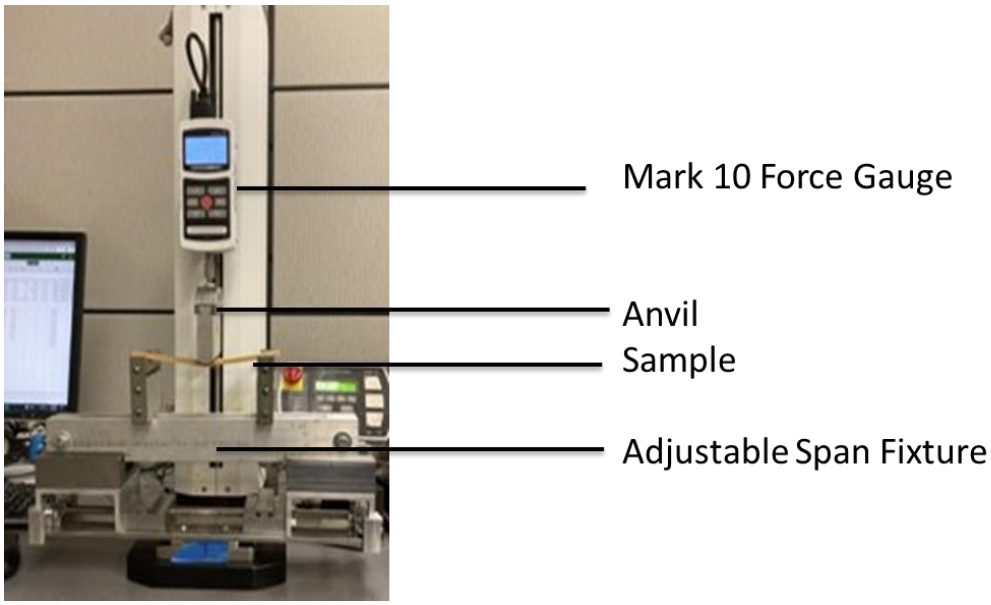

Figure 11. Flexural Test Setup

Figure 12. Flexural Tested Sample

3.5.6 Hardness Test

To measure the resistance of localized plastic deformation of a wood sample, hardness testing was conducted. ASTM D1037 standards were followed accordingly for the fixture and calculations (American Society for Tests and Materials, 2018). Samples were prepared, as shown in Figure 2. The samples were placed onto the Instron MTS fixture in Figure 13, modified for the Janka ball hardness test. Penetrations of the sample were made starting at the left end, at distance intervals of 51 mm, so that one penetration would not affect the other. Three penetrations were made for each treatment. The load at 5.6 mm penetration was recorded as the hardness. Penetrated samples are displayed in Figure 14.

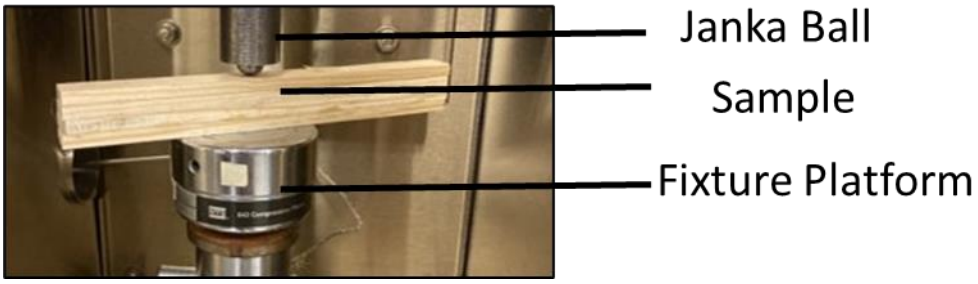

Figure 13. Hardness Test Setup

Figure 14. Hardness Tested Sample

3.5.7 Lap Shear Test

To evaluate the adhesive bonding strength of an SYP sample against shear forces, lap shear testing was conducted. ASTM D2339 standards were followed accordingly for the fixture and

calculations (American Society for Tests and Materials, 2018). Five SYP strips were cut into shorter 6.35 mm thick x 76 mm length x 17.50 mm width strips. These shorter strips were glued together from a single sample across a 25 mm length and 17.50 mm width using a Rehau 1B hot melt adhesive (Leesburg, VA) and clamped together on the center of the sample overnight. The sample was spread such that an even thickness of adhesive was distributed across the contact area between the two SYP strips. The resulting samples are displayed in Figures 15a and 15b.

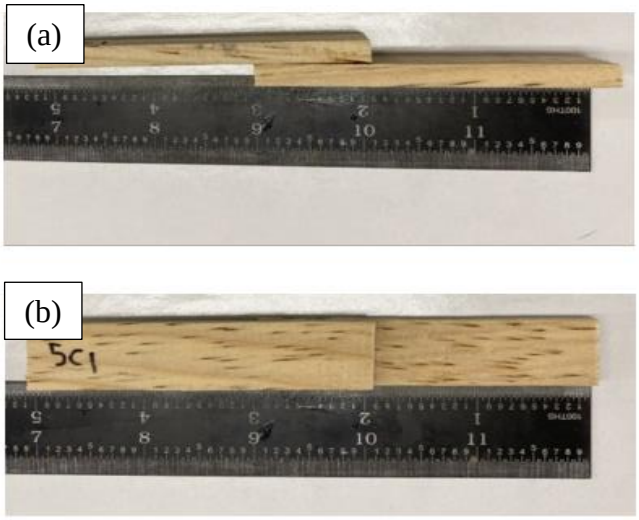

Figure 15. Lap Shear Test Sample (a) Side View and (b) Top View

The samples were then placed onto an Instron MTS equipped with a 30 kN tensile testing apparatus. These samples were set parallel to one another by a thin (3 mm thick) SYP sample, as displayed in Figure 16. The samples were then separated from one another at a rate of 1 mm/min as opposed to using the load control as suggested in the standard. The sample was tested until adhesive failure, where the maximum load was recorded such that the lap shear strength of the SYP could be calculated. The apparatus and loaded sample are displayed in Figure 16, while the tested sample is shown in Figure 17.

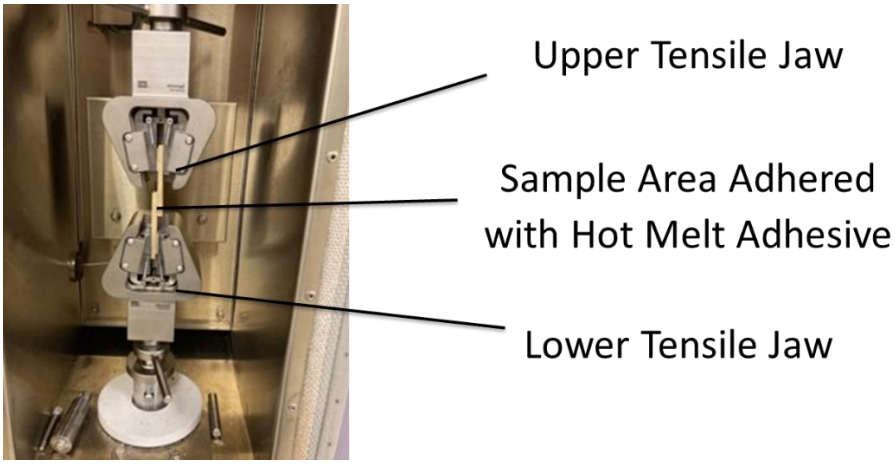

Figure 16. Lap Shear Test Setup

Lap shear was then calculated using the following equation:

$$\tau = \frac{F_{shear}}{wa} \qquad \text{(Equation 7)}$$

where τ is the shear strength (in MPa), F_{shear} is the shear force required to separate the samples (in N), w is the width of the sample (in mm), and a is the length of the glued pieces when bonded together (in mm).

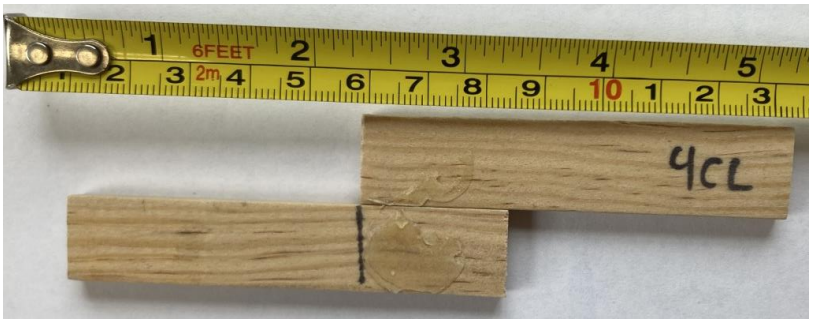

Figure 17. Lap Shear Tested Sample

3.5.8 Screw Withdrawal Test

To evaluate the various loads and ways in which screws fail under tension, the screw withdrawal test was conducted. ASTM D1037 standards were followed accordingly for the

fixture and calculations (American Society for Tests and Materials, 2018). Samples were prepared and marked following the same protocol as Figure 2, Section 3.2.1 (25 mm thick x 180 mm length x 17.50 mm width). A 3.2 mm diameter lead hole was drilled, followed by the drilling of the screw using a Phillips head screwdriver to prevent the stripping of the screws. A commercially purchased 16 threads-per-inch type AB wood screw with a root diameter of 3.5 mm was used for each test. This screw was aligned with two steel washers attached underneath the head, as shown in Figure 18. Screws were fastened starting at the left end of the sample at distance intervals of 51 mm so that one penetration would not affect the other at three different points of the sample. The screws were then withdrawn at a rate of 1.5 mm/min until the screw was removed. The peak force required to remove the screw was recorded. A resulting sample from the test is displayed in Figure 19.

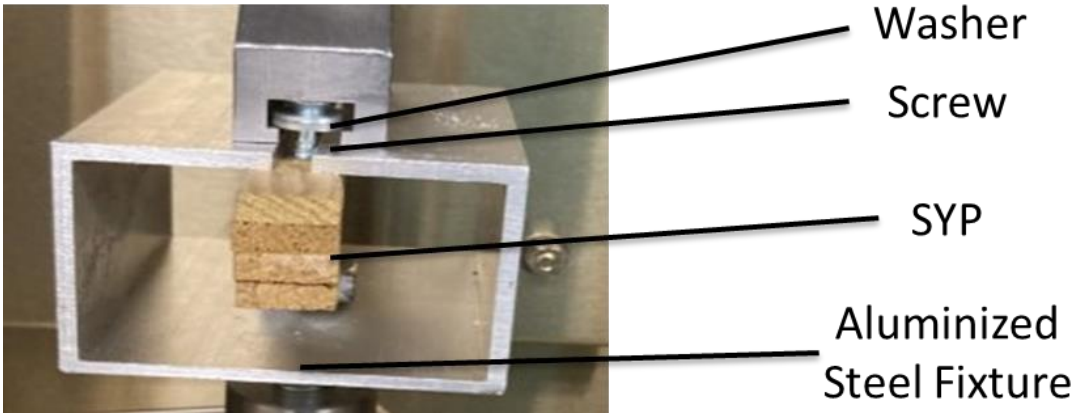

Figure 18. Screw Withdrawal Test Setup

Figure 19. Screw Withdrawal Tested Sample

3.5.9 Nail Withdrawal Test

To evaluate the ability of a wood sample to withdraw nails via tension, nail withdrawal testing was conducted. ASTM D1037 standards were followed accordingly for the fixture and calculations (American Society for Tests and Materials, 2018). Samples were prepared and marked as described in Figure 2, Section 3.2.1 (25 mm thick x 180 mm length x 17.50 mm width). A 6d nail with a 2.87 mm shank diameter and a 51 mm length was hammered 6.35 mm (the thickness of the specimen as manufactured) into the sample with a steel washer underneath the head. The sample was rested for 24 hours allowing for the wood to settle. The nail was then placed into a 30 kN Instron MTS force gauge at a rate of 1.5 mm/min, shown in Figure 20. The peak force to fully withdraw the nail and fracture mode was recorded. A nail withdrawal tested sample is displayed in Figure 21. Nails were driven starting at the left end of the sample at distance intervals of 51 mm so that one penetration would not affect the other. This process was repeated at three points in the sample.

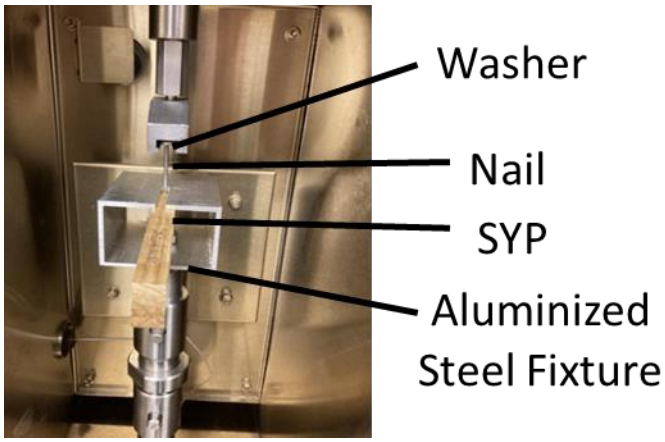

Figure 20. Nail Withdrawal Test Setup

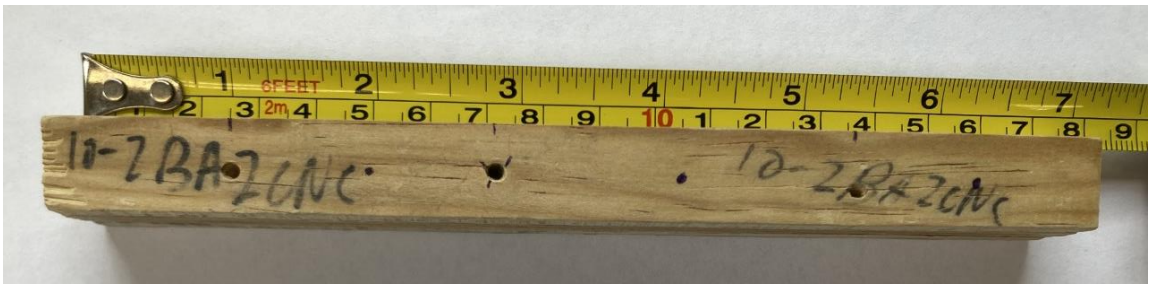

Figure 21. Nail Withdrawal Tested Sample

3.6 Statistical Analysis

Statistical analysis was conducted to discern patterns and trends in the data and remove potential biases from the evaluated data using numerical analysis. Minitab was the software used for statistical analysis in all tests and treatments. Simple statistical analysis and several Analysis of Variance (ANOVA) models were generated for the data to obtain objective results on each variable's effect on the response values considered to evaluate the hypotheses of the tests described in Chapter 3.

Simple statistical analysis calculations were conducted for standard deviation (SD) and coefficient of variation (CV). SD is a measure of the dispersion of data from the mean, with greater SD indicating greater spread in the data, which can be used to estimate the overall variation of a process. The calculation is displayed in the following equation:

$$\sigma = \sqrt{\frac{\sum(x-\bar{x})^2}{N}} \qquad \text{(Equation 8)}$$

where the symbol σ (sigma) is often used to represent the standard deviation of a population, $\bar{x}$ is the sample mean average, x is the collected sample value, and N is the sample size. (Montgomery et al., 2013).

The coefficient of variation (CV) is a standardized measure of the dispersion of a probability distribution or frequency distribution. CV was obtained to measure the variation of the data universally. It is expressed as a percentage, calculated automatically through Minitab, and this value was calculated using the following equation:

$$CV = \frac{\sigma}{\bar{x}} * 100 \qquad \text{(Equation 9)}$$

where CV represents the coefficient of variation, σ the standard deviation, and $\bar{x}$ the sample mean average.

3.6.1 Analysis of Variance

Analysis of variance (ANOVA) is a statistical model that can estimate experimental errors and the effect of changing variables within a design on a single response value for a specified confidence level. In this study, a multiple-factor ANOVA was conducted for all tests, and response data were in a separate column for each factor level to determine the statistical differences of each treatment. Equal variances were assumed at a 95% confidence interval.

The calculations of ANOVA comprise of computing several means and variances, dividing the two variances, and comparing the ratio to a handbook value to determine statistical significance. ANOVA estimates 3 sample variances: a total variance based on all the observed deviations from the grand mean, an error variance based on all the observed deviations from their appropriate treatment means, and a treatment variance. ANOVA models can be broken down into several estimated effect factors; main effects, interaction effects, and error effects, all of which are used to estimate how much of the provided variables account for the variability of the responses. Main effects estimate the amount of response change that is due solely to the level of a single variable changing, interaction effects account for the effect of the response from a

combination of changes in variable levels, and the error effect accounts for the randomness of the provided response values and also accounts for a possible lack of relevant variables that are included within the model.

Another critical value displayed in the ANOVA tables is the adjusted (or total) sum of squares (SS_A). The adjusted sum of squares is a measure that determines whether or not there is a statistically significant difference between the group means. SS_A is calculated via the treatment sum of squares (SS_R) and the error sum of squares (SS_E) in the following equation:

$$SS_A = SS_R + SS_E = N\sum(X_j - \bar{X})^2 + N\sum(X_{ij} - \bar{X}_j)^2 \qquad \text{(Equation 10)}$$

where N represents the samples size, X_j is the observed value of group j, X_{ij} is the *i*th observation in group j, $\bar{X}$ is the overall mean, and $\bar{X}_j$ is the mean of group j. The adjusted mean squares (MS_A) represent an estimate of the population variance. They are calculated by dividing the adjusted sum of squares by the degrees of freedom, as shown in the equation below:

$$MS_A = \frac{SS_A}{N} \qquad \text{(Equation 11)}$$

where MS_A is the adjusted mean square, SS_A is the adjusted sum of squares, and N is the sample size. The F statistic can be found to compare the factors of total deviation, and the F-test comparison to the F-distribution can be performed. The F statistic can be found by using the following equation:

$$F = \frac{variance\ between\ treatments}{variance\ within\ treatments} = \frac{MS_A}{MS_E} \qquad \text{(Equation 12)}$$

where F is the F statistic, MS_T represents the mean square for the pertinent factor T, and MS_E represents the mean squared error value. MS_E is calculated using the following equation:

$$MS_E = \frac{1}{n}\sum(Y_i - \bar{Y}_i)^2 \qquad \text{(Equation 13)}$$

where Y_i is the vector of observed values, and $\bar{Y}_i$ is the vector of predicted values. The F statistic is such that if the F value is greater than a characteristic F value based on the desired confidence level and degrees of freedom (df, calculated as the number of responses(n) -1) in the considered treatment group, there is a statistically significant difference between data sets. For the application in ANOVA, an F statistic for a specific factor greater than the characteristic F value means the factor has a statistically significant effect on the variation observed within the response values.

It should be noted that an equivalent p statistic in place of the F statistic when creating ANOVA tables is used in various statistical software packages. The p statistic is the probability of obtaining a test statistic that will take on a value at least as extreme as the observed value. The p-statistic is significant when the null hypothesis, the claim that no relationship exists between two data sets or variables being analyzed, is true. This value is based on the confidence interval, commonly 95%, and is the confidence interval in this thesis. The only difference with this statistic is that if a calculated p statistic for a certain factor is less than 1-α, where α is the confidence level, the factor significantly affects the response variable. As a result, if a p-value less than 0.05 is obtained in this study, the null hypothesis can be rejected, and thus, the results are statistically different.

3.6.1.1 Tukey Comparison Test. Due to the large number of treatments, the Tukey Honest Significant Difference (HSD) comparison test was conducted. That is because compared to other comparison tests, such as the Fisher Least Significant Difference (LSD) test, the Tukey HSD test minimizes the likelihood of a type-1 error in the results, indicating a difference where one does not exist in the data as there are a total of 22 different treatments and variation in wood due to

factors such as density and cut location (i.e., heartwood versus latewood). Tukey's Test is a single step multiple comparison procedure and statistical test that uses the t-distribution to compare all possible pairs of data sets within a group of data sets by first calculating a characteristic difference value in the following equation:

$$T_\alpha = q(a, f)\sqrt{MS_E} \qquad \text{(Equation 14)}$$

Where T_α is the characteristic Tukey's difference value, q (a, f) is a test statistic value based on the t-distribution, a is the number of factors or data sets considered in the comparison, and MS_E represents the mean squared error value. Grouping information was assorted by letter and means that did not share a letter were significantly different.

3.6.1.2 Dunnett's Multiple Comparison Test. The Dunnett's test is a multiple comparison ANOVA procedure developed to compare several treatments with a single control. If an interval contains zero, indicated by the sharing of the letter "A" there is no significant difference between the two means under comparison. A family-wise error rate is specified for all comparisons, and Dunnett's method accordingly determines the confidence levels for each comparison. Due to the generalized nature of the Tukey pairwise comparison, which considers all kinds of pairwise comparisons, the Dunnett's test is used as it addresses a special case of comparing multiple treatment groups with a single control group. The Dunnett's test yields narrower confidence intervals simultaneously to increase precision within the data, reducing the likelihood of a type 1 error.

4 RESULTS AND DISCUSSION

4.1 Characterization

4.1.1 Field Emission Scanning Electron Microscopy

FE-SEM characterization shows the cellular walls of a sample. The importance of this characterization is to visualize the partial collapse of the cell walls due to the delignification combined with the vacuum pressure treatment (Qian et al., 2019). Additionally, FE-SEM was hypothesized to distinguish the crystalline cellulose from the amorphous cellulose within the wood. However, the lack of magnification and distinguishable elemental composition presented hurdles in visualizing the CNC within the SYP. Images were taken at 383x magnification.

Figure 22a depicts the control sample appears to have disrupted cell walls while the cell walls in the treated samples have collapsed due to the delignification and vacuum pressure treatment. Additionally, the cell walls in the control sample in Figure 22a appear to have a rough, non-uniform structure, while the treated sample has a smooth, uniform structure in Figure 22b. A smoother structure in the FE-SEM suggests lignin removal in the SYP, which agrees with the literature (Sun et al., 2009). It was also observed that upon polishing the samples, resin from polishing filled the tracheids of the sample. This resin is distinguishable due to the scratch marks and patterns located within the tracheids of the sample (Tan et al., 2020) observed in both Figures 22a and 22b. Moreover, the holes in the cell walls indicate that the resin has not completely encased the wood; thus, voids in the sample were left unfilled.

As a result, these images indicate the impacts of the wood sample's delignification and densification. However, the CNCs could not be detected, likely because wood and CNCs contain

cellulose and have minuscule dimensions (10-15 nm width and 80-100 nm length). EDX imaging was also attempted to detect CNC via sulfur groups, as the CNCs were treated using sulfuric acid. However, the sulfur concentration was too low for EDX detection as the sulfur consisted of a fraction of an already low concentration of CNC. As a result, other characterization techniques had to be used to detect the presence of CNCs in the sample.

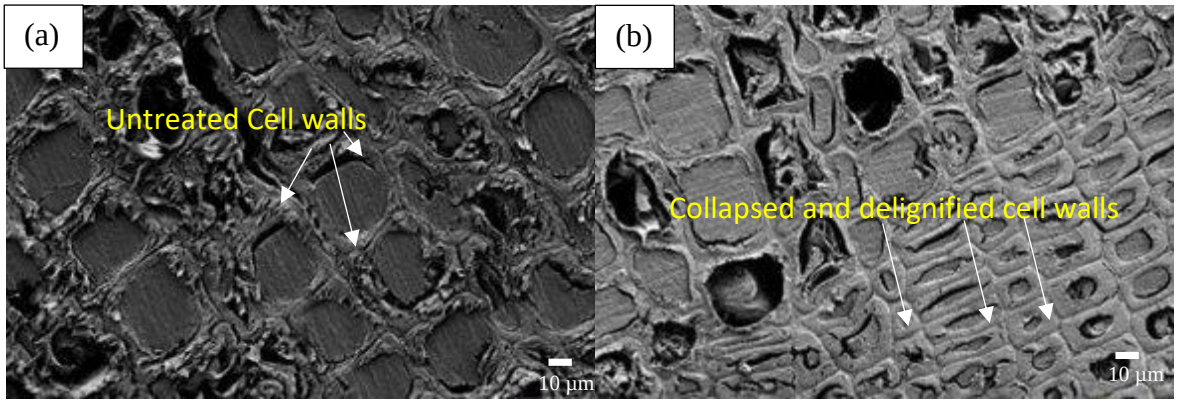

Figure 22. Field Emission Scanning Electron Microscopy Images of (a) Untreated (CL) and (b) Treated (3N2AA2CNC) Southern Yellow Pine Wood (Perpendicular to Grain)

4.1.2 Atomic Force Microscopy

Because of the nano-scale dimensions of CNCs, AFM was used to detect the presence of CNCs within a sample through modulus mapping and determine the impact that CNCs have on the mechanical properties of a sample. Current AFM imaging has generated 2D modulus maps with resolutions down to 1.5 nm of cellulosic nanomaterials (Wagner et al., 2016). Another study also produced AFM images that studied wood in a cement environment (Li et al., 2022). However, the novelty of this study lies in generation 3-dimensional maps of surface topography overlaid with monochromatic modulus maps shown for a control sample (Figure 23) and a 3N2AA2CNC treated sample (Figure 24). AFM characterization aimed to detect CNCs in the SYP due to the numerous additives and similar composition of CNCs to wood.

The detection of CNCs was partially supported via modulus mapping using the Hertzian contact model due to the extremely high stiffness of CNC relative to the SYP. Stiffness was marked on a monochromatic scale, where lower stiffness values are darker (~3-8 GPa), while higher stiffness values are lighter (~20 GPa). The untreated maps had an average modulus of 9.639 ± 4.284 GPa, whereas the 3N2AA2CNC sample had an average modulus of 10.351 ± 5.395 GPa.

These results allude to the detection possibilities of CNC using this technique. However, due to small size of the scanned surface, additional scans need to be conducted in order to provide sufficient support regarding the presence of CNC in the sample. Additionally, the stiffness on the map was found to be more evenly distributed, possibly due to delignification, as this is consistent with FE-SEM imaging described in Figure 22, which depicts the removal of the rough, nonuniform structure of the cell walls via delignification. However, if a surface has sharp protrusions, the Hertzian contact model becomes unstable, resulting in false areas of high stiffness. A similar phenomenon occurs in a 1998 paper by Stark et al. Here, the paper attempts to determine the MOE of an aerogel powder using the Hertzian contact model. However, it fails to model areas of rough inclusions. As a result, although there are areas of high stiffness on the sample in Figure 23, the areas were likely produced as a failure of the Hertzian contact model due to the drastic roughness of the untreated surface.

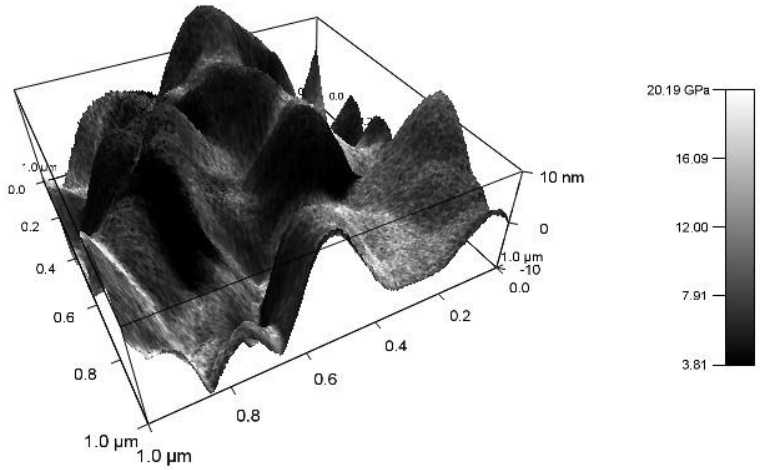

Figure 23. 3D Atomic Force Microscopy Elastic Modulus Map of Untreated (CL) Southern Yellow Pine Wood (Parallel to Grain)

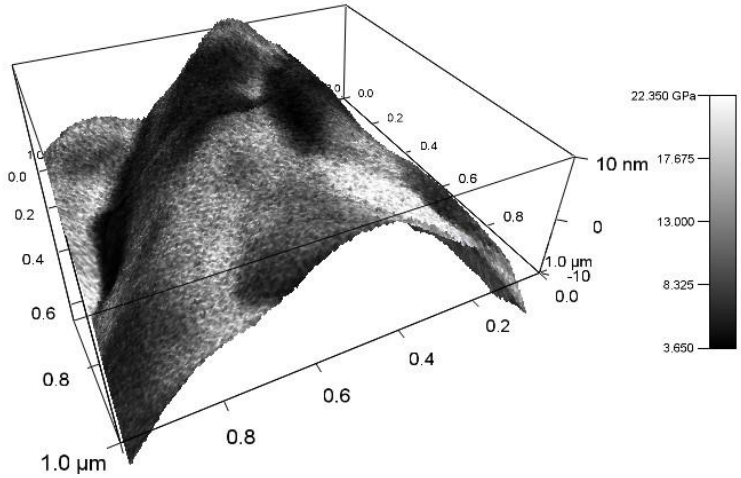

Figure 24. 3D Atomic Force Microscopy Elastic Modulus Map of Treated (3N2AA2CNC) Southern Yellow Pine Wood (Parallel to Grain)

4.1.3 Fourier-Transform Infrared Spectroscopy

Fourier transform infrared spectroscopy was used to determine changes in chemical composition in the SYP due to treatment. It was expected that ester groups and functional groups would be detected as a result of the 3N2BA2CNC and the 3N2AA2CNC treatments as the addition of these acids functionalized the surface of the CNC and were hypothesized to undergo

Fisher-Speier esterification. Additionally, the CL and the 2CNC were expected to contain groups that indicated the presence of lignin or other extractives in SYP as they did not undergo NaOH delignification.

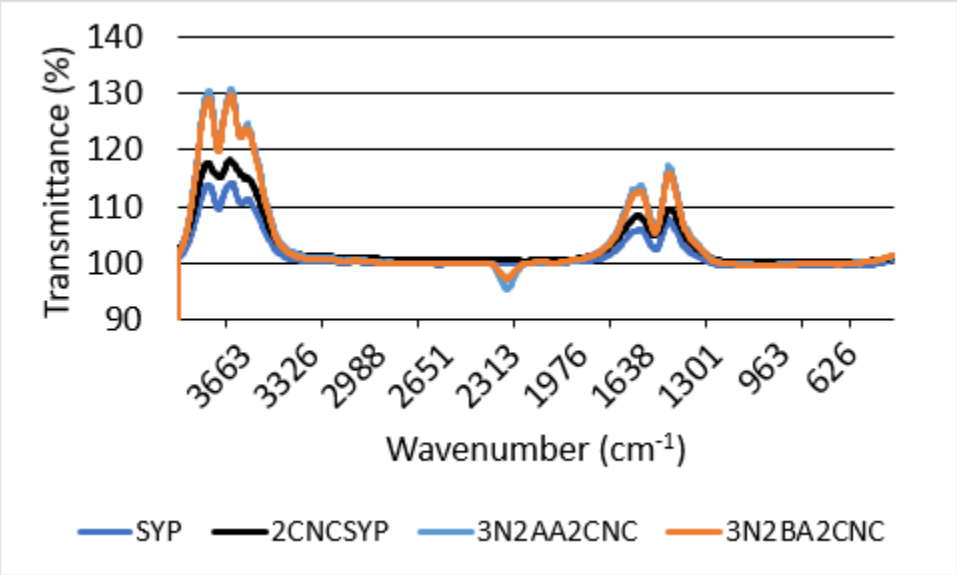

Figure 25: Fourier Transformation Infrared Spectroscopy: Wavenumber versus Transmittance of four Southern Yellow Pine Wood Treatments

The resulting FTIR spectra of these treatments were collected and included the wavenumbers from 500 cm^{-1} to 4000 cm^{-1} in Figure 25 with peaks described in a table by Larkin et al., 2017. Peaks were observed at 1218 cm^{-1} for the 3N2AA2CNC treatment, indicating the presence of ester groups likely the result of Fisher-Speier esterification. Similar peaks were not detected for the 3N2BA2CNC treated samples, likely due to the lack of solubility of the BA, inhibiting the esterification of the CNC. Peaks at 1600 – 1610 cm^{-1} were also detected due to the 3N2BA2CNC and 3N2AA2CNC treatment, indicating the presence of amino acid zwitterions, molecules that contain an equal number of positively and negatively charged functional groups (Chai et al., 2003). Peaks at 1520-1530 cm^{-1} and 1680-1690 cm^{-1} were found in the CL and 2CNC samples,

respectively, indicating the presence of wood extractives. The peaks at 1520-1530 cm^{-1} suggest the presence of aromatic nitrogen groups, while the peaks at 1680-1690 cm^{-1} suggest the presence of unsaturated aromatic acids (Miklečić et al., 2012).

4.2 Physical and Mechanical Properties Tests

4.2.1 Density

Density measurements and change in density tests were conducted using five samples from each formulation to evaluate the effects of delignification and the impregnation of CNC into the SYP (Section 3.5.1). There was strong evidence that CNC caused significantly higher changes in density ($p = 0.05$) by ANOVA (Table 4).

Table 4: Analysis of Variance: Change in Density

Source	DF	Adj SS	Adj MS	F-Value	P-Value
NaOH	1	11.22	11.22	0.06	0.807
CNC	2	2302.67	1151.34	6.22	0.005
AA	1	0.23	0.23	0	0.972
Error	30	5549.11	184.97		
Lack-of-Fit	1	72.92	72.92	0.39	0.539
Pure Error	29	5476.2	188.83		
Total	34	8170.54			

*The following terms cannot be estimated due to failing the regression test and were removed: BA

The delignified samples treated with functionalized CNC were expected to have the greatest density due to the pores being filled with CNCs, which have a density of 1600 kg/m^3 (Mariano et al., 2014), compared to commercially sourced SYP, which only has a density 476 kg/m^3. NaOH and AA treatments do not show statistically significant differences in density compared to the untreated SYP (Table 4) as their p-values are much greater than 0.05. Despite an

initial mass loss, delignification by NaOH has been found to have a minimal impact on the density of the SYP (Kuai et al., 2022).

Table 5 displays the mean density of each treatment along with their percentage changes and Tukey comparison. Values were obtained for seven formulations, including control. Control had 0% Δρ, SD, and CV because it was not treated. The 5% CNC treatment showed the greatest observed change in density (an increase of 29.96%), with a density of 600.52 kg/m3, and was the only treatment significantly different from the control sample (p-value < 0.05) according to the Tukey comparison correction. The density value of the 5% CNC treatment was comparable to that of American Beech and Sugar Maple (640.00 kg/m^3) as described in Table 1.

Table 5: Statistical Means with Tukey Comparison: Density

Treatment	Mean Density (kg/m^3)	Δρ (%)	SD	CV
5CNC	600.52	29.96^{A}	4.61	15.38
3N2BA2CNC	548.55	26.19^{AB}	3.72	14.22
3N2BA5CNC	587.00	24.71^{AB}	1.37	5.56
3N2AA2CNC	575.59	23.58^{AB}	3.52	14.91
2CNC	546.93	21.19^{AB}	1.18	5.55
3N2AA5CNC	548.55	16.67^{AB}	1.55	9.29
CL	476.50	0^{B}	0	0
3NVP	501.5858	1.81^{B}	0.30	14.47

*Means that do not share a letter are significantly different.

Testing conducted with a combination of delignification (3N) and a vacuum pressure treatment with water showed a 1.81% increase in density, which was deemed insignificant. However, this lack of change was the result of the masses and volumes of the 3NVP samples decreasing a similar percentage to one another (mass decreased by 6.20% and volume decreased by 7.90% with the 3NVP treatment). This indicates that the combination of delignification and vacuum pressure treatment causes a reduction in volume, likely as a result of the applied pressure

treatment on the SYP facilitating the collapse of the cell walls (Liang et al., 2022), consistent with Figure 22.

Table 6: Dunnett's Multiple Comparison: Change in Density

NaOH	N	Mean (%)	Grouping
0 (Control)	15	17.17	A
3	20	15.50	A
CNC	**N**	**Mean (%)**	**Grouping**
0 (Control)	5	0.72	A
5	10	27.33	
2	20	22.39	
AA	**N**	**Mean (%)**	**Grouping**
0 (Control)	25	16.21	A
2	10	16.45	A

*Means not labeled with the letter A are significantly different ($p < 0.05$) from the control level mean after multiple comparison corrections.

Since multiple treatments shared the same letters in the Tukey comparison test, the Dunnett multiple comparison test (shown in Table 6) was conducted to verify this effect. It was found that the CNC concentration had a significant effect with both 2% and 5% concentrations of added CNC. The results indicate a significant effect of CNC impregnation on the density of SYP. These results are supported when nano-aluminum oxide was impregnated into wood (Taghiyari et al., 2017), leading to an up to 10% increase in density only with impregnation. Moreover, it was observed that AA and BA functionalization did not have a significant effect on the density of the SYP, possibly due to the modification of the surface of the CNC reducing the hydrophilicity and hydrogen bonding density of the CNC, but not to a significant degree on the mass of the entire SYP system (Kamboj et al., 2022). One potential cause for the increased density of the SYP despite delignification is that the mass loss of lignin from the treatment of

SYP is mitigated by the additional CNC impregnation into the SYP. The increase in density as a result of impregnation is supported by a study on delignified and sodium silicate (a higher-density, higher strength material) impregnated poplar. Despite a 13% density growth ratio loss as a result of delignification, the poplar still exhibited a 32% density growth ratio when impregnated with sodium silicate (Kuai et al., 2022).

4.2.2 Water Absorption Test

Water absorption tests were conducted using five samples from each formulation, to determine the affinity of treated and untreated SYP samples to water. Water absorption of samples was measured at 24-hour periods as per ASTM D1037 specifications. The delignified samples treated with functionalized CNC were expected to have water absorption values similar to those of the untreated samples, despite CNCs being hydrophilic (Paskdel et al., 2021). Several studies have reported that functionalization with acetic acid and benzoic acid reduces the hydrophilicity of CNCs (Shikata et al., 2013). ANOVA was used to determine the significant differences between different formulations and factors (Table 7).

Table 7: Analysis of Variance: Water Absorption

Source	DF	Adj SS	Adj MS	F-Value	P-Value
N	1	80.261	80.261	9.40	0.005
CNC	2	361.781	180.891	21.18	0.000
AA	1	16.778	16.778	1.96	0.171
Error	30	256.180	8.539		
Lack-of-Fit	2	7.111	3.556	0.40	0.674

*The following terms cannot be estimated due to failing the regression test and were removed: BA

Table 7 shows the water absorption values of seven formulations, including control. The results show samples with 5% CNC had the highest water absorption (41.41%), whereas

delignified samples treated with BA functionalized samples had the lowest (30.25%). It was found that at higher CNC concentrations, water absorption increases slightly, possibly due to the hydrophilic properties of CNC (Shikata et al., 2013), as displayed in Table 6, resulting in an increase from 36.85% to 41.14%.

Table 8: Statistical Means with Tukey Comparison: Water Absorption

Treatment	N	Mean (%)	SD	CV
5CNC	5	41.14^{A}	1.76	4.27
3N2AA5CNC	5	39.45^{AB}	1.27	3.21
3N2BA5CNC	5	38.32^{AB}	1.38	3.60
CL	5	36.85^{AB}	1.74	4.72
2CNC	5	35.45^{BC}	0.86	2.42
3N2AA2CNC	5	31.41^{C}	1.58	5.03
3N2BA2CNC	5	30.25^{C}	1.82	3.26

*Means that do not share a letter are significantly different.

Due to the sharing of multiple letters in the Tukey comparison test, the Dunnett's multiple comparison test shown in Table 8 was conducted to verify this effect. It was found that NaOH led to a significant decrease in water absorption from (38.39% to 34.76%). This observation indicates the possibility that sodium hydroxide treatment led to the collapse of the cell walls, hindering the transport of water in the cells, hence the SYP's reduced water absorption. The effect of delignification reducing water absorption is supported by a previous study, where delignification facilitated the collapse of cell walls (Liang et al., 2022), making it difficult to absorb water. As a result, water absorption decreased from 36.85% to 30.25% due to the 3N2BA2CNC treatment (Wang et al. 2021). Table 9 indicated CNCs had a significant effect at the 5% concentration level due to the hydrophilicity of CNC (Shikata et al., 2013) resulting in an increase from 35.77% to 40.67%. Another observation from table 8 noted that neither AA nor BA had an effect in reducing the moisture absorption of the CNC, despite the esterification of the

CNC. Table 9 supports this by sharing a letter in the Dunnett's test. The presence of this observation is an indicator that there may be more variables that may need to be controlled to produce the differences in water absorption as a result of the surface functionalization of CNC.

Table 9: Dunnett's Multiple Comparison: Water Absorption

NaOH	N	Mean (%)	Grouping
0 (Control)	15	38.39	A
3	20	34.76	
CNC	**N**	**Mean (%)**	**Grouping**
0 (Control)	5	35.77	A
2	15	33.75	A
5	15	40.67	
AA	**N**	**Mean (%)**	**Grouping**
0 (Control)	25	35.81	A
2	10	37.65	A

*Means not labeled with the letter A are significantly different ($p < 0.05$) from the control level mean after multiple comparison corrections.

4.2.3 Thickness Swelling

Thickness swelling tests were conducted using five samples from each formulation to determine the volumetric affinity of treated and untreated SYP samples to water. The thickness swelling of samples was measured at 24-hour periods as per ASTM D1037 specifications. The delignified samples and those treated with functionalized CNC were expected to have values similar to that of the untreated samples despite the hydrophilic nature of CNCs (Paskdel et al., 2021). Several studies have reported that functionalization with acetic acid and benzoic reduces the hydrophilicity of wood (Shikata et al., 2013), while delignification enhances the dimensional stability of the SYP (Kuai et al., 2022). ANOVA was used to determine the significant differences between different formulations and factors (Table 10). It was observed that

significant changes occurred strongly as a result of delignification and there appears to be weak evidence that CNC treatment resulted in significant changes to thickness swelling of the SYP.

Table 10: Analysis of Variance: Thickness Swelling

Source	DF	Adj SS	Adj MS	F-Value	P-Value
N	1	47.318	47.3180	15.15	0.001
CNC	2	16.759	8.3794	2.68	0.085
AA	1	5.251	5.2509	1.68	0.205
Error	30	93.688	3.1229		
Lack-of-Fit	2	0.238	0.1192	0.04	0.965
Pure Error	28	93.450	3.3375		
Total	34	194.523			

*The following terms cannot be estimated due to failing the regression test and were removed: BA

Table 11 shows the thickness swelling values of seven formulations, including the control. The results show samples with 5% CNC had the highest water thickness swelling (10.398 %), whereas delignified samples treated with AA functionalized samples had the lowest thickness swelling (5.205%). It was found that at higher CNC concentrations, the thickness increases slightly due to the hydrophilic properties of CNC, as displayed in Table 11, from 8.258% to 10.398%.

Table 11: Statistical Means with Tukey Comparison: Thickness Swelling

Treatment	N	Mean (%)	SD	CV
5CNC	5	10.398^{A}	1.22	12.91
2CNC	5	9.450^{AB}	0.82	11.33
CL	5	8.258^{ABC}	0.53	8.25
3N2BA5CNC	5	7.256^{ABC}	0.39	7.39
3N2BA5CNC	5	6.443^{ABC}	0.10	4.10
3N2AA5CNC	5	6.440^{BC}	0.63	19.80
3N2AA2CNC	5	5.205^{C}	0.70	13.42

*Means that do not share a letter are significantly different.

Due to the sharing of multiple letters in the Tukey comparison test among several samples, the Dunnett's multiple comparison test shown in Table 12 was conducted to verify treatment effects. There appears to be no evidence that the CNC concentration affected the thickness swelling as SYP, as they shared the same Dunnett's test letter in Table 12. However, an increase from 6.207% to 8.375% in thickness swelling from the control level to level 5 in the CNC treatment in Table 12 was observed, indicating that there is a minuscule change as a result of the hydrophilicity of CNC, but not that of a significant degree. Another notable observation from Table 12 is that a significant decrease in thickness swelling from 8.858% to 5.781% as a result of delignification. This observation alludes to the possibility that sodium hydroxide treatment led to the collapse of the cell walls obstructing water transport, hence the SYP's reduced thickness. The effect of delignification also reducing thickness swelling is supported by a previous study, where delignification facilitated the collapse of cell walls (Liang et al., 2022), making it difficult for the wood to swell. causing overall thickness swelling to decrease from 8.258% to 5.205% as a result of the 3N2AA2CNC treatment (Wang et al. 2021).

Table 12: Dunnett's Multiple Comparison: Thickness Swelling

NaOH	**N**	**Mean (%)**	**Grouping**
0 (Control)	15	8.858	A
3	20	5.781	
CNC	**N**	**Mean (%)**	**Grouping**
0 (Control)	5	6.207	A
2	15	7.376	A
5	15	8.375	A
AA	**N**	**Mean (%)**	**Grouping**
0 (Control)	25	7.832	A
2	10	6.810	A

*Means not labeled with the letter A are significantly different ($p < 0.05$) from the control level mean after multiple comparison corrections.

Another observation noted is that neither AA nor BA had an effect in reducing the moisture absorption of the CNC, as the BA failed the linear regression test, and observations in Tables 10 and 12 support this due to its p-value of greater than 0.05 and sharing a letter in the Dunnett's test. This observation indicates that more variables may need to be controlled to produce the differences in thickness swelling.

4.2.4 Linear Expansion

Linear expansion testing was conducted to determine the relative expansion of SYP in the lengthwise dimension due to changes in environmental humidity. Samples that underwent linear expansion testing were measured at 24-hour periods at 50% humidity and 90% humidity as per ASTM D1037 specifications. The delignified and functionalized CNC-treated samples were expected to have values similar to that of the untreated samples due to delignified and densified poplar wood having enhanced dimensional stability. Moreover, several studies have indicated that functionalization with acetic acid and benzoic reduces the hydrophilicity of wood (Shikata et al., 2013).

Table 13: Analysis of Variance: Linear Expansion

Source	DF	Adj SS	Adj MS	F-Value	P-Value
NaOH	1	0.020	0.020	1.810	0.189
CNC	2	0.048	0.024	2.190	0.129
AA	1	0.006	0.006	0.590	0.450
Error	30	0.327	0.011		
Lack-of-Fit	1	0.004	0.004	0.370	0.548
Pure Error	29	0.323	0.011		
Total	34	0.420			

*The following terms cannot be estimated due to failing the regression test and were removed: BA

ANOVA was used to determine the significant differences between different formulations and factors (Table 13). Table 14 indicated Tukey testing that all formulations shared the same letter, displaying no sign of significant differences between any of the formulas. The lack of significance is further supported by ANOVA findings in Table 13 showing all treatments having p-values greater than 0.05.

Table 14: Statistical Means and Tukey Comparison: Linear Expansion.

Treatment	Linear Expansion (%)	SD	CV
CL	0.344^{A}	0.066	13.91
2CNC	0.398^{A}	0.061	16.65
5CNC	0.484^{A}	0.070	14.51
3N2AA2CNC	0.317^{A}	0.075	14.27
3N2BA2CNC	0.343^{A}	0.067	19.42
3N2AA5CNC	0.341^{A}	0.057	17.89
3N2BA5CNC	0.345^{A}	0.049	13.67

*Means that do not share a letter are significantly different.

Due to a lack of significant differences, a Dunnett's test was also conducted in Table 15, which detected no significant difference between levels as well.

Table 15: Dunnett's Multiple Comparison: Linear Expansion

NaOH	N	Mean (%)	Grouping
0 (Control)	15	0.389	A
3	20	0.318	A
CNC	**N**	**Mean (%)**	**Grouping**
0 (Control)	5	0.289	A
5	10	0.414	A
2	20	0.357	A
AA	**N**	**Mean (%)**	**Grouping**
0 (Control)	25	0.373	A
2	10	0.334	A

*Means not labeled with the letter A are significantly different ($p < 0.05$) from the control level mean after multiple comparison corrections.

The lack of notable differences combined with the drastic value changes observed in some groups in the Dunnett's method led to the development of a model-reduced ANOVA table (Table 16), removing AA to discount its effects as it had the highest p-value of 0.450. These results indicate that the NaOH treatment caused a significant change in linear expansion as a p-value less than 0.05 was obtained.

Table 16: Model Reduced Analysis of Variance: Linear Expansion

Source	DF	Adj SS	Adj MS	F-Value	P-Value
NaOH	1	5.54E-02	5.54E-02	5.15	0.030
CNC	2	4.20E-02	2.10E-02	1.95	0.159
Error	31	3.33E-01	1.07E-02		
Lack-of-Fit	1	8.29E-03	8.29E-03	0.77	0.388
Pure Error	30	3.25E-01	1.08E-02		
Total	34	4.20E-01			

Following the reduced-ANOVA table in Table 16, the Dunnett's multiple comparison test was conducted and displayed in Table 17. The reduced-Dunnett's multiple comparison found that NaOH significantly reduced linear expansion from 0.41% to 0.31% from factor levels 0 to 3. A probable cause of this decrease was the delignification facilitating the collapse of the cell walls during vacuum pressure treatment. This result is supported by several studies that indicate that delignification facilitates the collapse of the cell walls of poplar (Liang et al., 2022 and Luo et al., 2022), hindering water transport throughout the sample. Table 17 also observed that there were no significant changes in linear expansion into SYP as a result of CNC impregnation, despite an increase from 0.301% to 0.412%, further supported by a Table 15, which produced a p-value of 0.159. A likely reason for the difficulty in detecting significant increases in linear

expansion is the variation between samples shown in Table 14 as high coefficient of variation values were observed (<10%).

Table 17: Model Reduced Dunnett's Multiple Comparison: Linear Expansion

NaOH	N	Mean (%)	Grouping
0 (Control)	15	0.414	A
3	20	0.312	
CNC	**N**	**Mean (%)**	**Grouping**
0 (Control)	5	0.301	A
5	20	0.412	A
2	20	0.373	A

*Means not labeled with the letter A are significantly different ($p < 0.05$) from the control level mean after multiple comparison corrections.

4.2.5 Flexural Test

Flexural tests were conducted on ten samples from each formulation to determine the stiffness and bending strengths of treated and untreated SYP samples. MOR and MOE were measured and calculated as per ASTM D1037 specifications as described in section 3.5.5. All treatments were expected to lead to a significant increase in MOR and MOE as NaOH would open the pores of the SYP, allowing for superior penetration of CNCs upon vacuum pressure treatment, which has superior mechanical properties (tensile strength: 7 GPa elastic moduli of 150 GPa, and crystallinity: 54–88%) (Habibi et al., 2014). This is supported by a study that indicate that the insertion of CNC into wood increases its MOE and MOR (Luo et al., 2022). The addition of AA or BA was expected to strengthen the CNCs further as previous studies have found superior crystallinity (from 64% to 80-83%) and dispersion with AA functionalization (Tang et al., 2013) and superior Young's modulus (an increase of 20%) with BA (Shojaeiarani et al., 2018)

4.2.5.1 Modulus of Rupture The modulus of rupture represents the maximum flexural strength the SYP undergoes before failure. Table 18 displays an ANOVA table of the treatments and their interactions, indicating strong evidence to reject the null hypothesis that CNC and BA caused significant changes to the MOR due to obtaining p-values ~ 0.000 and 0.008, respectively. Additionally, there was weak evidence to reject the null hypothesis that AA causes significant changes to MOR as the obtained p-value lied between 0.05-0.10, while for NaOH, there was no evidence to reject the null hypothesis due to the observation of a p-value of 0.358, alluding that delignification did not enhance the stiffness of SYP.

Table 18: Analysis of Variance: Modulus of Rupture

Source	DF	Adj SS	Adj MS	F-Value	P-Value
NaOH	1	7.46E+02	7.46E+02	0.85	0.358
CNC	3	9.48E+04	3.16E+04	35.92	0.000
AA	1	3.36E+03	3.36E+03	3.82	0.052
BA	1	6.21E+03	6.21E+03	7.06	0.008
Error	233	2.05E+05	8.80E+02		
Lack-of-Fit	17	5.72E+04	3.36E+03	4.91	0
Pure Error	216	1.48E+05	6.85E+02		
Total	239	3.19E+05			

Table 19 shows the MOR values of seven formulations, their statistical means, and Tukey comparison. The results indicate that all treatments differed significantly and increased relative to the control, as they did not share a letter except for the 3N2BA5CNC treatment, which shared the letter C with the control. Moreover, the 2CNC treatment had the highest observed MOR of 171.12 MPa, superior to that of Live Oak by a difference of 35% (Table 1). Due to the letter

sharing among numerous treatments, the Dunnett's test was also conducted for further analysis of the effects of each treatment as a result of NaOH, CNC, AA, and BA treatment (Table 20).

Table 19: Statistical Means and Tukey Comparison: Modulus of Rupture

Treatment	Mean (MPa)	SD	CV
2CNC	171.12^{A}	21.36	12.48
5CNC	169.55^{A}	20.85	13.85
3N2AA5CNC	162.68^{AB}	14.45	8.88
3N2BA2CNC	156.50^{AB}	23.80	15.31
3N2AA2CNC	150.54^{AB}	15.38	11.9
3N2BA5CNC	129.27^{BC}	9.33	5.5
CL	102.42^{C}	21.4	20.9

*Means that do not share a letter are significantly different.

Table 20 shows the Dunnett's test observations of treated and untreated SYP. It was observed that the addition of CNC led to a significant increase in MOR, while BA led to a significant decrease in MOR. A possible reason for the decrease in MOR is the lack of dispersion of the BA functionalized CNC due to its lack of solubility (Jasmani et al., 2016), thus hindering nano dispersion during ultrasonication. On the other hand, an increase from 124.74 MPa to 133.91 MPa was observed with AA. This is likely due to the acetylation of the CNCs improving the dispersion and crystallinity of CNC throughout the SYP (Tang et al., 2013). Another notable observation is CNCs may have enhanced MOR by penetrating into the SYP, which is supported by a previous study reported increases in MOR due to impregnating poplar wood with high MOR materials such as CNC and nano-aluminum-oxide due to its superior mechanical strength (Taghiyari et al., 2017 and Luo et al., 2022).

Table 20: Dunnett's Multiple Comparison: Modulus of Rupture

N	N	Mean (MPa)	Grouping
0 (Control)	120	127.56	A
3	120	131.09	A
CNC	**N**	**Mean (MPa)**	**Grouping**
0 (Control)	60	97.18	A
2	60	147.54	
5	60	143.99	
AA	**N**	**Mean (MPa)**	**Grouping**
0 (Control)	160	124.74	A
2	80	133.91	A
BA	**N**	**Mean (MPa)**	**Grouping**
0 (Control)	160	135.55	A
2	80	123.09	

*Means not labeled with the letter A are significantly different ($p < 0.05$) from the control level mean after multiple comparison corrections.

4.2.5.2 Modulus of Elasticity The modulus of elasticity represents the sample's stiffness during initial loading before unrecoverable deformation occurs. Table 21 displays an ANOVA table constructed of the treatments and their interactions. The ANOVA table contains strong evidence that significant differences were observed with the BA and AA treatments due to their p-values being significantly less than 0.05, approaching zero.

Table 21: Analysis of Variance: Modulus of Elasticity

Source	DF	Adj SS	Adj MS	F-Value	P-Value
N	1	1.76E+07	1.76E+07	1.86	0.174
CNC	3	9.51E+08	3.17E+08	33.49	0.000
AA	1	1.02E+08	1.02E+08	10.73	0.001
BA	1	8.05E+06	8.05E+06	0.85	0.357
Error	224	2.12E+09	9.47E+06		
Lack-of-Fit	8	1.64E+08	2.05E+07	2.27	0.024
Pure Error	216	1.96E+09	9.05E+06		
Total	239	3.36E+09			

Table 22 shows the MOE values of seven formulations, including the control. The results show samples with the 3N2AA2CNC treatment having the highest MOE of 19580 MPa, while the 3N2BA5CNC had the lowest MOE of 17206 MPa, superior to that of Live Oak, which has an MOE of 13700 MPa, a 43% increase (Table 1). There also appears to be a pattern where MOE CNC at 5% CNC appeared to have a lower value than 2CNC. Moreover, numerous treatments appear to share letters, indicating more analysis needs to be conducted to verify the differences.

Table 22: Statistical Means and Tukey Comparison

Treatment	Mean (MPa)	SD	CV
3N2AA2CNC	19580^{A}	3579	18.28
3N2AA5CNC	18396^{AB}	1380	7.50
5CNC	18015^{AB}	1643	9.12
3N2BA2CNC	18013^{AB}	3982	22.11
2CNC	17412^{AB}	2832	16.26
3N2BA5CNC	17206^{ABC}	2649	15.40
CL	11419^{C}	1827	16.00

*Means that do not share a letter are significantly different.

Due to the sharing of multiple letters in the Tukey comparison test among several samples, the Dunnett's multiple comparison test shown in Table 23 was conducted to verify treatment effects. The Dunnett's test indicated that CNC did have a significant effect on the MOE of a sample as they shared a letter. Additionally, a slight decrease in hardness was observed at the 5% CNC concentration, hinting at the possibility that CNCs began to localize on the surface due to the increased viscosity of the solution. A study found a decrease in the hardness of CNC at higher solution concentrations, causing CNC localization on the surface

(Mohamed et al., 2018). Additionally, it was found that AA appeared to have a significant increase in CNC, possibly as a result of surface functionalization (Rana et al., 2021). Another noted observation was that delignification with NaOH did not appear to have a significant impact on improving the mechanical properties of CNC due to having a p-value greater than 0.05 in Table 21 while sharing a letter in Table 22. However, NaOH was expected to enhance the mechanical properties of the SYP, as there was an observed increase of 542 MPa in the mean MOE was observed in Table 23, hinting at the possibility of an increase as delignification was expected to enhance the impregnation outcomes with CNC due to similar observations with poplar wood (Luo et al., 2022). Based on these results, more factors may affect the modulus of elasticity than were accounted for in the initial design of the experiment, indicating more variables may need to be controlled to produce the desired modulus of elasticity for the NaOH treatment.

Table 23: Dunnett's Multiple Comparison: Modulus of Elasticity

N	**N**	**Mean (MPa)**	**Grouping**
0 (Control)	120	15622	A
3	120	16164	A
CNC	**N**	**Mean (MPa)**	**Grouping**
0 (Control)	60	12057	A
2	60	18582	
5	60	18119	
AA	**N**	**Mean (MPa)**	**Grouping**
0 (Control)	160	15096	A
2	80	16689	
BA	**N**	**Mean (MPa)**	**Grouping**
0 (Control)	160	16117	A
2	80	15668	A

*Means not labeled with the letter A are significantly different ($p < 0.05$) from the control level mean after multiple comparison corrections.

4.2.6 Hardness Test

Hardness tests were conducted to measure resistance to localized plastic deformation of a wood sample. CNC treatment was expected to increase the hardness, while the functionalization of CNC with BA or AA would further increase the hardness due to the conversion of surface hydroxyls into esters, improving CNC dispersion of the sample, while NaOH would not affect hardness. This is supported by studies that indicate related properties such as the ultimate strength of PLA thermoplastic, strengthened by BA functionalized CNC (Shojaeiarani et al., 2018), possibly improving hardness values and a study finding that delignified wood fiber-polypropylene found no changes in hardness upon delignification (Karimi et al., 2006). ANOVA was used to determine the significant differences between different formulations and factors. Table 24 displays an ANOVA table of the hardness test, which indicates that only BA and CNC resulted in a significant change due to having p-values less than 0.05, whereas NaOH and AA did not result in a significant change.

Table 24: Analysis of Variance: Hardness Test

Source	DF	Adj SS	Adj MS	F-Value	P-Value
NaOH	1	2670	2670	0.03	0.872
CNC	2	797809	398905	3.95	0.028
BA	1	1004304	1004304	9.95	0.003
Error	37	3736113	100976		
Lack-of-Fit	1	1511020	1511020	24.45	0
Pure Error	36	2225093	61808		
Total	41	5593304			

*The following terms cannot be estimated due to failing the regression test and were removed: AA

Table 25 displays the statistical means and Tukey comparison of the data. This data indicates strong evidence that the 3N2AA2CNC and 2CNC treatments significantly differ from

the control sample due to them not sharing a letter with the CL treatment. It was also found that despite having a greater mean, the 3N2BA2CNC was found not to share the letter C with the control, indicating somewhat of a decrease as a result of the BA contradicting the expected results.

Table 25: Statistical Means and Tukey Comparison: Hardness Test

Treatment	Mean (N)	SD	CV
3N2AA2CNC	3598^{A}	217.7	6.05
2CNC	3437^{AB}	43.3	1.26
5CNC	3143^{BC}	70.6	2.32
3N2AA5CNC	2501^{C}	168.6	6.74
3N2BA5CNC	2822^{CD}	194.2	6.88
CL	2814^{CD}	110.1	3.91
3N2BA2CNC	2996^{D}	204.6	6.83

*Means that do not share a letter are significantly different.

The Dunnett's multiple comparison test was used to further verify the efficacy of the treatments in Table 26 due to its limited likelihood of attaining a type-1 error. It was found through the Dunnett's multiple comparison test that BA caused a significant decrease in the hardness of SYP due to the lack of a shared letter. A possible cause of this is a lack of dispersion of the BA functionalized CNC due to its lack of solubility (Jasmani et al., 2016), thus hindering nano dispersion during ultrasonication. CNC was also observed to have caused a significant increase in hardness. The means obtained via the Dunnett's test for CNC found a significant difference between CNC levels 0 wt. % compared to the 2 and 5 wt.%. However, the addition of CNC from 2 to 5 wt.% CNC does not increase as greatly as from 0 to 2 wt. % CNC. A possible cause for this is the increased viscosity of the solution, leading to the localization of CNC on the surface of the SYP. A previous study that studied the microhardness of CNC-reinforced resin

found that the 4% CNC had a slightly greater hardness compared to 6% when dispersed throughout a polyester and measured at a 5 N load for hardness (Mohamed et al., 2018).

Table 26: Dunnett's Multiple Comparison: Hardness Test

NaOH	N	Mean (N)	Grouping
0 (Control)	9	2870	A
3	12	2893	A
CNC	**N**	**Mean (N)**	**Grouping**
0 (Control)	3	2597	A
5	6	3078	
2	12	2970	
BA	**N**	**Mean (N)**	**Grouping**
0 (Control)	15	3110	A
2	6	2653	

*Means not labeled with the letter A are significantly different ($p < 0.05$) from the control level mean after multiple comparison corrections.

4.2.7 Lap Shear Test

Lap shear tests were conducted using five samples from each formulation to determine the adhesive bonding strength of an SYP sample against shear forces. Lap shear tests were measured and calculated as per ASTM D1037 specifications. NaOH delignification was expected to decrease lap shear due to the formation of microcracks onto the SYP, likely due to delignification, resulting in lower shear strength (Dimitriou et al., 2018). Functionalized CNC with either BA or AA was expected to mitigate this decrease due to its ability to enhance the interfacial adhesion of polymers such as PLA-PHB (Arrieta et al., 2014). Moreover, acetylation of CNC with AA was expected improve CNC dispersion (Tang et al., 2013) throughout the SYP, improving its lap shear. ANOVA determined the significant differences between different formulations and factors (Table 27).

Table 27: Analysis of Variance: Lap Shear

Source	DF	Adj SS	Adj MS	F-Value	P-Value
N	1	16.453	16.453	540.94	0.000
CNC	2	8.1269	4.0635	133.6	0.000
AA	1	0.4805	0.4805	15.8	0.000
Error	30	0.9125	0.0304		
Lack-of-Fit	2	0.4691	0.2346	14.82	0.000
Pure Error	28	0.4433	0.0158		
Total	34	25.0028			

**The following terms cannot be estimated due to failing the regression test and were removed: BA

Table 27 displays seven formulations' statistical means and Tukey comparison values, including control. The results show the 5CNC treatment yielded the highest lap shear (4.308 MPa), while the 3N2BA2CNC yielded the lowest (1.842 MPa). It was found that higher concentrations in CNC led to greater lap shear, with 5CNC having a lap shear of 4.31 MPa. CNCs likely increased lap shear due to their short (<100 nm), rigid, and rod-like morphology, which increased the shear strength of epoxy adhesive from 14-40 MPa (Lee et al., 2021).

Table 28: Statistical Means and Tukey Comparison: Lap Shear

Treatment	Lap Shear (MPa)	SD	CV
5CNC	4.31^{A}	0.10	3.28
2CNC	3.64^{B}	0.14	3.35
3N2AA5CNC	3.06^{C}	0.10	4.10
CL	3.03^{C}	0.11	5.70
3N2BA5CNC	2.48^{D}	0.05	1.67
3N2AA2CNC	1.88^{E}	0.19	10.23
3N2BA2CNC	1.842^{E}	0.14	3.80

*Means that do not share a letter are significantly different.

Due to the variation in letter grouping of different treatments, the Dunnett's multiple comparison test shown in Table 28 was conducted to verify treatment effects. There appears to be strong evidence that CNC, NaOH, and AA had a significant effect on lap shear as they did not share a letter in the Dunnett's test and had p-values of approximately zero, while BA was not included due to its failure of the regression test. There was an observed decrease in lap shear due to NaOH, possibly due to the caustic nature of NaOH impairing the fibers on the surface of the wood (Rajeshkumar et al., 2021). Additionally, it was found that AA also improves the lap shear of samples, likely due to the AA esterification of CNC and improved dispersion of CNC with AA via acetylation (Tang et al., 2013). The improvement of lap shear using AA is supported by a study that found that esterified CNCs increased the lap shear of various plastic films (Fotie et al., 2020). BA did not appear to have a significant effect on lap shear as it failed the regression test, likely due to its lack of solubility (Jasmani et al., 2016), hindering nano-dispersion during ultrasonication.

Table 29: Dunnett's Multiple Comparison: Lap Shear

NaOH	**N**	**Mean (MPa)**	**Grouping**
0 (Control)	15	3.82	A
3	20	2.00	
CNC	**N**	**Mean (MPa)**	**Grouping**
0 (Control)	5	2.28	A
5	15	3.64	
2	15	2.81	
AA	**N**	**Mean (MPa)**	**Grouping**
0 (Control)	25	2.75	A
2	10	3.06	

*Means not labeled with the letter A are significantly different ($p < 0.05$) from the control level mean after multiple comparison corrections.

4.2.8 Screw Withdrawal Test

Screw withdrawal tests were conducted using five samples from each formulation to determine the various loads in which screws fail under tension. Screw withdrawal tests were measured and calculated as per ASTM D1037 specifications. NaOH was expected to cause a decrease in screw withdrawal due to the loss of lignin but an increase when combined with AA or BA functionalized CNC due to their increased crystallinity and excellent mechanical properties (Fotie et al., 2020). ANOVA analysis was used to determine the significant differences between different formulations and factors (Table 30).

Table 30: Analysis of Variance: Screw Withdrawal

Source	DF	Adj SS	Adj MS	F-Value	P-Value
NaOH	1	3.71E+05	3.71E+05	28.76	0.000
CNC	2	2.97E+04	1.49E+04	1.15	0.341
BA	1	2.16E+04	2.16E+04	1.68	0.214
Error	16	2.06E+05	1.29E+04		
Lack-of-Fit	1	3.34E+04	3.34E+04	2.9	0.109
Pure Error	15	1.73E+05	1.15E+04		
Total	20	7.29E+05			

*The following terms cannot be estimated due to failing the regression test and were removed: AA

Table 31 displays screw withdrawal values of seven formulations, including control. It was found that the 3N2BA5CNC treatment yielded the greatest screw withdrawal (1373 N), while the 5CNC sample yielded the lowest screw withdrawal (894 N). No significant changes in screw withdrawal occurred as a result of CNC impregnation. However, combined with delignification, massive increases in screw withdrawal were observed. To confirm this observation, Dunnett's testing had to be conducted (Table 32).

Table 31: Statistical Analysis and Tukey Comparison: Screw Withdrawal

Treatment	Mean (N)	SD	CV
3N2BA5CNC	1373^{A}	46.2	3.36
3N2AA5CNC	1298^{AB}	73.4	5.65
3N2AA2CNC	1122^{BC}	45.0	4.01
3N2BA2CNC	1100^{BCD}	109.5	9.95
CL	947^{CD}	118.7	12.54
2CNC	907^{D}	11.0	1.21
5CNC	894^{D}	59.9	6.70

*Means that do not share a letter are significantly different.

Due to the sharing of multiple letters in the Tukey comparison test among several samples, the Dunnett's multiple comparison test shown in Table 32 was conducted to verify treatment effects. There appears to be strong evidence that the delignification via NaOH led to a significant increase in the screw withdrawal of SYP, from 868 N to 1262 N, as they did not share a letter in Table 32, and a p-value less than 0.05 was observed in Table 30. The significant increase occurred, likely because delignification compressed the cell walls and enhanced the CNC penetration into the wood, increasing the overall hardness of the sample, while simply CNC impregnation lacked thorough penetration. The same could not be observed for CNC and AA, as they shared a letter in Table 32 with a p-value greater than 0.05. Moreover, BA was excluded as it failed the regression test and could not be estimated. These results indicate that delignification had a significant effect, increasing the mean screw withdrawal in Table 32. This possibility is supported by the fact that the 3N2BA2CNC and 2CNC treatments did not share a letter in Table 31. Additionally, in a study where poplar wood was delignified and impregnated with furfuryl resin, delignification alone decreased the dimensional stability of poplar and collapsed the cell walls. However, when combined with furfuryl resin treatment, the compression

of the cell walls and the impregnation of furfuryl resin caused increased uniformity in the microstructure (Yang et al., 2019).

Table 32: Dunnett's Multiple Comparison: Screw Withdrawal

NaOH	N	Mean (N)	Grouping
0 (Control)	9	869	A
3	12	1262	
CNC	**N**	**Mean (N)**	**Grouping**
0 (Control)	3	1096	A
5	6	1096	A
2	12	1004	A
BA	**N**	**Mean (N)**	**Grouping**
0 (Control)	15	1113	A
2	6	1018	A

*Means not labeled with the letter A are significantly different ($p < 0.05$) from the control level mean after multiple comparison corrections.

4.2.9 Nail Withdrawal Test

Nail withdrawal tests were conducted using five samples from each formulation to determine the loads in which nails fail under tension. Nail withdrawal tests were conducted as per ASTM D1037 specifications. NaOH was expected to decrease in nail withdrawal due to lignin loss but an increase when combined with AA or BA functionalized CNC due to delignification improving the penetration of the CNC nanosuspension, which has increased crystallinity and excellent mechanical properties relative to the SYP (Fotie et al., 2020 and Luo et al., 2022). ANOVA determined significant differences between different formulations and factors (Table 33). The ANOVA table found significant changes only as a result of NaOH delignification.

Table 33: Analysis of Variance: Nail Withdrawal

Source	DF	Adj SS	Adj MS	F-Value	P-Value
NaOH	1	806.67	806.667	4.56	0.049
CNC	2	157.33	78.667	0.44	0.649
BA	1	0.27	0.267	0	0.97
Error	16	2833.33	177.083		
Lack-of-Fit	1	48	48	0.26	0.619
Pure Error	15	2785.33	185.689		
Total	20	4642.57			

*The following terms cannot be estimated due to failing the regression test and were removed: AA

Table 34 shows the nail withdrawal values of seven formulations, including the control. It was found that the 3N2AA2CNC treatment yielded the greatest nail withdrawal (66 N), while the 5CNC sample yielded the lowest nail withdrawal (32 N). No significant changes in nail withdrawal occurred as a result of CNC impregnation. However, combined with delignification, massive increases in nail withdrawal were observed.

Table 34: Statistical Means and Tukey Comparison: Nail Withdrawal

Treatment	Mean (N)	SD	CV
3N2AA2CNC	66.00^{A}	5.16	7.82
3N2BA2CNC	56.00^{AB}	5.08	9.07
3N2BA5CNC	54.67^{ABC}	2.52	4.60
3N2AA5CNC	49.33^{ABC}	1.53	3.10
CL	42.67^{BC}	3.06	7.16
2CNC	41.33^{BC}	9.61	23.25
5CNC	32.00^{C}	2.65	8.27

*Means that do not share a letter are significantly different.

Due to the sharing of multiple letters in the Tukey comparison test among several samples, the Dunnett's multiple comparison test shown in Table 35 was conducted to verify

treatment effects. There appears to be strong evidence that the delignification via NaOH had a significant effect on the thickness swelling as SYP, increasing the mean nail withdrawal from 38.83 N to 57.16 N in Table 35, as they did not share a letter and a p-value less than 0.05 was observed in Table 33. The same could not be observed for CNC and BA, as they shared a letter in Table 35 with a p-value greater than 0.05 in Table 33. Moreover, AA was excluded as it failed the regression test and could not be estimated. The reason that the NaOH had a significant effect is likely due to delignification enhancing the penetration of CNC throughout the sample. A study where poplar wood was delignified and impregnated with furfuryl resin found that delignification alone decreased the dimensional stability of poplar and collapsed the cell walls. However, when combined with furfuryl resin treatment, the compression of the cell walls and the resin made the poplar wood dimensionally stable (Yang et al., 2019).

Table 35: Dunnett's Multiple Comparison: Nail Withdrawal

NaOH	**N**	**Mean (N)**	**Grouping**
0 (Control)	9	38.83	A
3	12	57.16	
CNC	**N**	**Mean (N)**	**Grouping**
0 (Control)	3	52.00	A
2	12	48.67	A
5	6	43.33	A
BA	**N**	**Mean (N)**	**Grouping**
0 (Control)	15	47.83	A
2	6	48.17	A

*Means not labeled with the letter A are significantly different ($p < 0.05$) from the control level mean after multiple comparison corrections.

5 CONCLUSIONS

The objectives of this project were: to optimize and validate an effective process of impregnating wood with functionalized CNCs and determine critical variables influencing CNC impregnation into the wood; to investigate the microstructural, physiological, and compositional changes in wood impregnated with CNC; and to evaluate the physical and mechanical properties of CNC-impregnated wood.

The first objective was completed using a solution-based alkali delignification technique that increased the porosity of wood to enhance CNC impregnation. Delignification was followed by an ultrasonication technique where an aqueous solution of functionalized CNC was introduced into a chamber for even nanodispersion and impregnation into the wood. It was found that ultrasonication impregnated the wood with CNCs while evenly dispersing the CNC nanodispersion. The samples were then transferred into another vessel for vacuum pressure impregnation to remove the air pockets and impregnate additional CNC into the wood using a CNC solution.

The second objective was completed through FTIR, AFM, and FE-SEM. Microstructural and morphological changes of the modified SYP were analyzed using FE-SEM, localized surface properties of the SYP were examined using AFM, and the chemical compositional changes were detected through FTIR. The investigation observed the collapse of the cell walls and lignin removal through FE-SEM. AFM detected the presence of CNC in the sample through modulus mapping and provided additional surface topography data. FTIR detected the presence of functional groups and ester groups within the functionalized CNC-modified SYP.

The third objective was completed through a series of ASTM D1037 and ASTM D2339 tests. The results found improvements in some physical properties (reduced water absorption from 36.85% to 30.25% and thickness swelling from 8.258% to 5.205%) (Tables 7 & 10, respectively) and some mechanical properties (increased MOR from 102.42 MPa to 171.12 MPa and MOE from 11419 MPa to 19580 MPa) (Tables 17 & 20, respectively).

Overall, this study has shown that the combination of CNC's delignification, densification, and impregnation has proven to increase certain mechanical properties such as MOR and MOE, resulting in a 68% and 72% increase, respectively. Delignification enhanced fastener withdrawal properties with little to no effect on moisture absorption properties. On the other hand, other properties, such as lap shear (decrease from 3.03 MPa to 1.88 MPa) (Table 26), were inhibited by this process. CNC vacuum-pressure impregnation had positive effects, such as increased fastener withdrawal resistance, MOR, MOE, and lap shear strength. Overall, it appears that the addition of CNC into SYP has the potential to be a high-strength engineering material comparable to that of high-strength hardwood species, resulting in potential advanced architectural or engineering applications such as cross-laminated timber and hardwood flooring. It was found that the best wood impregnation treatment was 3N2AA2CNC. Further improvements could be made in the treatment process by adding a heat compression densification treatment of the wood samples to reduce water absorption and a uniform microstructure (Taghiyari et al., 2017).

Moreover, a novel method for CNC detection was developed using AFM. It has been discovered that the use of a box cutter to prepare samples for AFM mapping is a simple, effective technique that prevented the risk of resin contamination and the work required for

surface polishing. Clusters of CNCs concentrated in certain points of a 1 μm^2 sample, along with the smoothening of the SYP surface due to delignification. Future work includes additional testing to determine the impregnation efficiency of wood due to the small mass of CNC being impregnated into the wood prevents significant differences from being detected; industrialization of the wood impregnation process, such as the use of this material in CLT, and as the use of AFM could only provide an estimate of CNC impregnation on a small area of the wood, finding a method to cut SYP samples smoothly to provide maps of larger areas across a wood sample would greatly improve the images produced. There is also the possibility that alternative wood impregnation techniques, such as the Lowry method, may be more suitable for impregnating CNCs as a direct impregnation technique. Preliminary research observed at a 110% increase in MOE and an 86% increase in MOR values through the replications of the 3N2AA2CNC treatment.

REFERENCES CITED

Alanis, Andrés, et al. "Plasma surface-modification of cellulose nanocrystals: A green alternative towards mechanical reinforcement of ABS." *RSC advances* 9.30 (2019): 17417-17424.

Ameh, J. O., S. Aliu, and S. Oyediran. "Acceptability and use of innovative bamboo products for the construction of residential buildings in Nigeria." *Architecture* 10.4 (2019).

American Society for Testing and Materials. *Annual Book of ASTM Standards*, Section 4, vol. 04.09-Wood, Philadelphia, PA. (2018).

Angles, M. Neus, and Alain Dufresne. "Plasticized starch/tunicin whiskers nanocomposite materials. 2. Mechanical behavior." *Macromolecules* 34.9 (2001): 2921-2931.

Arrieta, Marina Patricia, et al. "Multifunctional PLA–PHB/cellulose nanocrystal films: processing, structural and thermal properties." *Carbohydrate polymers* 107 (2014): 16-24.

Babiak, Marián, et al. "Modulus of elasticity in three-and four-point bending of wood." *Composite Structures* 204 (2018): 454-465.

Balasbaneh, Ali Tighnavard, and Willy Sher. "Comparative sustainability evaluation of two engineered wood-based construction materials: Life cycle analysis of CLT versus GLT." *Building and Environment* 204 (2021): 108112.

Bhanthumnavin, W., P. Wanichapichart, W. Taweepreeda, S. Sirijarukula, and B. Paosawatyanyong. Surface modification of bacterial cellulose membrane by oxygen plasma treatment. *Surface and Coatings Technology*, Vol. 306 (2016) pp. 272–278.

Blanchet, Pierre, Alizera Kaboorani, and Cecilia Bustos. "Understanding the effects of drying methods on wood mechanical properties at ultra and cellular levels." *Wood and Fiber Science* 48.2 (2016): 117-128.

Blanchette, Robert A. "Delignification by wood-decay fungi." *Annual review of phytopathology* 29.1 (1991): 381-403.

Brandner, Reinhard, et al. "Cross laminated timber (CLT): overview and development." *European Journal of Wood and Wood Products* 74 (2016): 331-351.

Briggs, David. "Enhancing forest value productivity through fiber quality." *Journal of Forestry* 108.4 (2010): 174-182.

Chanda, Saptaparni, and Dilpreet S. Bajwa. "A review of current physical techniques for dispersion of cellulose nanomaterials in polymer matrices." *Reviews on Advanced Materials Science* 60.1 (2021): 325-341.

Chanda, Saptaparni, et al. "Silane compatibilization to improve the dispersion, thermal and mechanical properties of cellulose nanocrystals in poly (ethylene oxide)." *Nanocomposites* 7.1 (2021): 87-96.

Chen, Jialin, et al. "Wood vessel-confined anti-swelling hydrogel for efficient osmotic energy conversion." *Nano Energy* 104 (2022): 107981.

Chen, Yao, et al. "Weathering characteristics of wood plastic composites reinforced with extracted or delignified wood flour." *Materials* 9.8 (2016): 610.

Couturaud, B., A. Baldo, A. Mas, and J. J. Robin. “Improvement of the interfacial compatibility between cellulose and poly(L-lactide) films by plasma-induced grafting of L-lactide: the evaluation of the adhesive properties using a peel test.” *Journal of Colloid and Interface Science*, Vol. 448 (2015): 427–436.

Dimitriou, Athanasios, M. D. Hale, and M. J. Spear. "The effect of pH on surface activation of wood polymer composites (WPCs) with hydrogen peroxide for improved adhesion." *International Journal of Adhesion and Adhesives* 85 (2018): 44-57.

Elazzouzi-Hafraoui, Samira, Jean-Luc Putaux, and Laurent Heux. "Self-assembling and chiral nematic properties of organophilic cellulose nanocrystals." *The Journal of Physical Chemistry B* 113.32 (2009): 11069-11075.

Esteves, Bruno. "Wood modification by heat treatment: A review." *BioResources* (2009): 370-404.

Fotie, Ghislain, et al. "Implementation of high gas barrier laminated films based on cellulose nanocrystals for food flexible packaging." *Applied Sciences* 10.9 (2020): 3201.

Mariano, Marcos, Nadia El Kissi, and Alain Dufresne. "Cellulose nanocrystals and related nanocomposites: Review some properties and challenges." *Journal of Polymer Science Part B: Polymer Physics* 52.12 (2014): 791-806.

Miklečić, Josip, Nikola Španić, and Vlatka Jirouš-Rajković. "Wood color changes by ammonia fuming." *BioResources* 7.3 (2012): 3767-3778.

Nur Izreen Farah, A., et al. "Improved performance of wood polymer nanocomposite impregnated with metal oxide nanoparticle-reinforced phenol formaldehyde resin." *Journal of Tropical Forest Science* 33.1 (2021): 77-87.

Forsgren, Lilian, et al. "Composites with surface-grafted cellulose nanocrystals (CNC)." *Journal of Materials Science* 54.4 (2019): 3009-3022.

Frey, Marion, et al. "Delignified and densified cellulose bulk materials with excellent tensile properties for sustainable engineering." *ACS Applied Materials & Interfaces* 10.5 (2018): 5030-5037.

Guan, Zhongwei, et al. "Structural characteristics of beam-column connections using compressed wood dowels and plates." *Proceedings of the World Conference on Timber Engineering (WCTE), Trentino (Italy)*. (2010).

Gindl, W., et al. "Mechanical properties of spruce wood cell walls by nanoindentation." *Applied Physics A* 79 (2004): 2069-2073.

Gwon, Jae Gyoung, et al. "Effects of chemical treatments of hybrid fillers on the physical and thermal properties of wood plastic composites." *Composites Part A: Applied Science and Manufacturing* 41.10 (2010): 1491-1497.

Habibi, Youssef. "Key advances in the chemical modification of nanocelluloses." *Chemical Society Reviews* 43.5 (2014): 1519-1542.

Habibi, Y., L. A. Lucia, and O. J. Rojas. “Cellulose nanocrystals: chemistry, self-assembly, and Applications.” *Chemical Reviews*, Vol. 110, No. 6, (2010): 3479–3500.

Habibi, Youssef, et al. "Bionanocomposites based on poly (ε-caprolactone)-grafted cellulose nanocrystals by ring-opening polymerization." *Journal of Materials Chemistry* 18.41 (2008): 5002-5010.

Hein, Paulo Ricardo Gherardi, and Loïc Brancheriau. "Comparison between three-point and four-point flexural tests to determine wood strength of Eucalyptus specimens." *Maderas. Ciencia y tecnología* 20.3 (2018): 333-342.)

Jakob, Matthias, et al. "The strength and stiffness of oriented wood and cellulose-fiber materials: A review." *Progress in Materials Science* 125 (2022): 100916.

Kamboj, Gourav, et al. "Effect of cellulose nanofiber and cellulose nanocrystals reinforcement on the strength and stiffness of PVAc bonded joints." *Composite Structures* 295 (2022): 115821.

Kamboj, Gourav, et al. "Comparative study on the properties of cellulose nanofiber (CNF) and cellulose nanocrystals (CNC) reinforced 1C-PUR adhesive bonded wooden joints." *Construction and Building Materials* 344 (2022): 128262.

Jasmani, Latifah, et al. "One-pot functionalization of cellulose nanocrystals with various cationic groups." *Cellulose* 23.6 (2016): 3569-3576.

Kane, Brian. "Withdrawal resistance of J-lags from three hardwood species." *Arboriculture and Urban Forestry* 37.3 (2011): 139.

Kargarzadeh H, Mariano M, Huang J, et al. “Recent developments on nanocellulose reinforced polymer nanocomposites: a review.” *Polymer*. (2017); 132: 368–393.

Karimi, Alinaghi, et al. "Effect of the delignification of wood fibers on the mechanical properties of wood fiber–polypropylene composites." *Journal of Applied Polymer Science* 102.5 (2006): 4759-4763.

Kollmann, Franz FP, Edward W. Kuenzi, and Alfred J. Stamm. “Principles of wood science and technology: II wood-based materials.” *Springer Science & Business Media* (2012).

Khakalo, Alexey, et al. "Delignification and ionic liquid treatment of wood toward multifunctional high-performance structural materials." *ACS applied materials & interfaces* 12.20 (2020): 23532-23542.

Kuai, Bingbin, et al. "Development of densified wood with high strength and excellent dimensional stability by impregnating delignified poplar by sodium silicate." *Construction and Building Materials* 344 (2022): 128282.

Lamouroux, Emmanuel, and Yves Fort. "An overview of nanocomposite nanofillers and their functionalization." *Spectroscopy of polymer nanocomposites* (2016): 15-64.

Laks, Peter E. "Wood Preservative Fungicides and the American Wood Preservers' Association Use Category System." *Development of Commercial Wood Preservatives* (2008): 228-240.

Lee, Koon-Yang, et al. "High-performance cellulose nanocomposites: comparing the reinforcing ability of bacterial cellulose and nanofibrillated cellulose." *ACS applied materials & interfaces 4.8* (2012): 4078-4086.

Leng, Weiqi, John F. Hunt, and Mehdi Tajvidi. "Screw and nail withdrawal strength and water soak properties of wet-formed cellulose nanofibrils bonded particleboard." *BioResources* 12.4 (2017): 7692-7710.

Li, Huayang, et al. "A green steam-modified delignification method to prepare low-lignin delignified wood for thick, large highly transparent wood composites." *Journal of Materials Research* 34.6 (2019): 932-940.

Li, Juan, and Bohumil Kasal. "The immediate and short-term degradation of the wood surface in a cement environment measured by AFM." *Materials and Structures* 55.7 (2022): 179.

Li, Jianguo, et al. "In situ wood delignification toward sustainable applications." *Accounts of Materials Research* 2.8 (2021): 606-620.

Li, Tian, et al. "Anisotropic, lightweight, strong, and super thermally insulating nanowood with naturally aligned nanocellulose." *Science Advances* 4.3 (2018): eaar3724.

Liang, Yunyi, et al. "Synthesis of ultra-high strength structured material from steam-modified delignification of wood." *Journal of Cleaner Production* 351 (2022): 131531.

Lin, Ning, et al. "Effects of polymer-grafted natural nanocrystals on the structure and mechanical properties of poly (lactic acid): A case of cellulose whisker-graft-polycaprolactone." *Journal of Applied Polymer Science* 113.5 (2009): 3417-3425.

Lin, Ning, et al. "Surface acetylation of cellulose nanocrystal and its reinforcing function in poly (lactic acid)." *Carbohydrate Polymers* 83.4 (2011): 1834-1842.

Littunen, Kuisma, et al. "Free radical graft copolymerization of nanofibrillated cellulose with acrylic monomers." *Carbohydrate polymers* 84.3 (2011): 1039-1047.

Lou, Zhichao, et al. "Synthesis of magnetic wood with excellent and tunable electromagnetic wave-absorbing properties by a facile vacuum/pressure impregnation method." *ACS Sustainable Chemistry & Engineering* 6.1 (2018): 1000-1008.

Luo, Honggang, et al. "Preparing the reinforced wood via embedding cellulose nanocrystals (CNC) into delignified fast-growing wood followed by densification." *Cellulose* 29.13 (2022): 7377-7396.

Manik, Parlindungan, Sarjito Joko Sisworo, and Good Rindo. "Technical and economic analysis of the usages glued laminated of Apus and petung bamboo as an alternative material component of timber shipbuilding." *Materials Today: Proceedings* 13 (2019): 115-120.

Marathe, Bhupesh, and Abhishek Kantak. "Nano additives: a review." *Paintindia* 58.7 (2008).

Matouk, Zineb, et al. "Functionalization of cellulose nanocrystal films using Non-Thermal Atmospheric–Pressure plasmas." *Applied Surface Science* 511 (2020): 145566.

Mekonnen, Tizazu H., Tesfaalem Haile, and Malin Ly. "Hydrophobic functionalization of cellulose nanocrystals for enhanced corrosion resistance of polyurethane nanocomposite coatings." *Applied Surface Science* 540 (2021): 148299.

Missoum, K., M. N. Belgacem, and J. Bras. “Nanofibrillated cellulose surface modification: a review.” *Materials, Vol. 6, No. 5* (2013): 1745–1766.

Mohamed, Yasser S., Hassan El-Gamal, and Moustafa Mahmoud Y. Zaghloul. "Micro-hardness behavior of fiber reinforced thermosetting composites embedded with cellulose nanocrystals." *Alexandria engineering journal* 57.4 (2018): 4113-4119.

Montgomery, D. C. "Montgomery: design and analysis of experiments." *John Willy & Sons* (2017).

Moon, Robert J., et al. "Cellulose nanomaterials review: structure, properties and nanocomposites." *Chemical Society Reviews* 40.7 (2011): 3941-3994.

Nepal, Prakash, Craig MT Johnston, and Indroneil Ganguly. "Effects on global forests and wood product markets of increased demand for mass timber." *Sustainability* 13.24 (2021): 13943.

Neto, Wilson Pires Flauzino. “Morphological investigation of cellulose nanocrystals and nanocomposite applications.” *Diss. Universidade Federal de Uberlândia*, (2017).

Nikolic, Miroslav, John Mark Lawther, and Anand Ramesh Sanadi. "Use of nanofillers in wood coatings: a scientific review." *Journal of Coatings Technology and Research* 12 (2015): 445-461.

Qian, Moriko, et al. "Optimization of delignification from Douglas fir sawdust by alkaline pretreatment with sodium hydroxide and its effect on structural and chemical properties of lignin and pyrolysis products." *Bioresource Technology Reports* 8 (2019): 100339.

Rajeshkumar, G., et al. "Influence of sodium hydroxide (NaOH) treatment on mechanical properties and morphological behaviour of Phoenix sp. fiber/epoxy composites." *Journal of Polymers and the Environment* 29 (2021): 765-774.

Rana, Ashvinder Kumar, Elisabete Frollini, and Vijay Kumar Thakur. "Cellulose nanocrystals: Pretreatments, preparation strategies, and surface functionalization." *International Journal of Biological Macromolecules* 182 (2021): 1554-1581.

Richter, K., et al. "Performance of cellulose nanofibrils in wood adhesives." *Proceedings of the Swiss Bonding, Rapperswil* (2009): 239-246.

Ross, Robert J. "Wood handbook: wood as an engineering material." *Forest Products Laboratory, Department of Agriculture Forest Service, Madison, Wisconsin, USA* (2021).

Sandberg, Dick, Andreja Kutnar, and George Mantanis. "Wood modification technologies-a review." *Iforest-Biogeosciences and forestry* 10.6 (2017): 895.

Schaefer, Dale W., and Ryan S. Justice. "How nano are nanocomposites?" *Macromolecules* 40.24 (2007): 8501-8517.

Shams, Md Iftekhar, Hiroyuki Yano, and Keijirou Endou. "Compressive deformation of wood impregnated with low molecular weight phenol formaldehyde (PF) resin III: effects of sodium chlorite treatment." *Journal of wood science* 51.3 (2005): 234-238.

Shen, Xiulun, et al. "Application of carboxylated cellulose nanocrystals as eco-friendly shale inhibitors in water-based drilling fluids." *Colloids and Surfaces A: Physicochemical and Engineering Aspects* 627 (2021): 127182.

Shikata, Toshiyuki, and Misumi Okuzono. "Are all polar molecules hydrophilic? Hydration numbers of ketones and esters in aqueous solution." *The Journal of Physical Chemistry B* 117.25 (2013): 7718-7723.

Shojaeiarani, Jamileh, Dilpreet S. Bajwa, and Nicole M. Stark. "Green esterification: A new approach to improve thermal and mechanical properties of poly (lactic acid) composites reinforced by cellulose nanocrystals." *Journal of applied polymer science* 135.27 (2018): 46468.

Sotayo, Adeayo, et al. "Review of state of the art of dowel laminated timber members and densified wood materials as sustainable engineered wood products for construction and building applications." *Developments in the Built Environment* 1 (2020): 100004.

Stark, Robert W., et al. "Determination of elastic properties of single aerogel powder particles with the AFM." *Ultramicroscopy* 75.3 (1998): 161-169.

Sun, Ning, et al. "Complete dissolution and partial delignification of wood in the ionic liquid 1-ethyl-3-methylimidazolium acetate." *Green Chemistry* 11.5 (2009): 646-655.

Ooi, Shok Yin, Ishak Ahmad, and Mohd Cairul Iqbal Mohd Amin. "Cellulose nanocrystals extracted from rice husks as a reinforcing material in gelatin hydrogels for use in controlled drug delivery systems." *Industrial Crops and Products* 93 (2016): 227-234.

Taghiyari, Hamid R., Ghonche Rassam, and Kazem Ahmadi-DavazdahEmam. "Effects of densification on untreated and nano-aluminum-oxide impregnated poplar wood." *Journal of forestry research* 28.2 (2017): 403-410.

Taj, Mohammad Ali, Saeed Kazemi Najafi, and Ghanbar Ebrahimi. "Withdrawal and lateral resistance of wood screw in beech, hornbeam, and poplar." *European Journal of Wood and Wood Products* 67.2 (2009): 135-140.

Tan, Bo, et al. "Pretreatment using diluted epoxy adhesive resin solution for improving bond strength between steel and wood surfaces." *International Journal of Adhesion and Adhesives 98* (2020): 102502.

Tang, Lirong, et al. "Ultrasonication-assisted manufacture of cellulose nanocrystals esterified with acetic acid." *Bioresource technology* 127 (2013): 100-105.

Taschuk, M. T., M. H. Matthew, M. J. Brett. “Handbook of deposition technologies for films and coatings.” *Elsevier* (2010): 621–678.

Toumpanaki, Eleni, Darshil U. Shah, and Stephen J. Eichhorn. "Beyond what meets the eye: Imaging and imagining wood mechanical–structural properties." *Advanced Materials* 33.28 (2021): 2001613.

Wagner, Ryan, Robert J. Moon, and Arvind Raman. "Mechanical properties of cellulose nanomaterials studied by contact resonance atomic force microscopy." *Cellulose* 23 (2016): 1031-1041.

Walker, John CF, Kevin Archer, and Stan Lebow. "Wood preservation." *Primary wood processing: principles and practice* (2006): 297-338.

Wang, Jiajun, et al. "Characterization of microstructure, chemical, and physical properties of delignified and densified poplar wood." *Materials* 14.19 (2021): 5709.

Wang, Junfeng, et al. "Effects of the combination of compression and impregnation with phenolic resin on the dimensional stability in the multiscale wood structure of Chinese fir." *Construction and Building Materials* 327 (2022): 126960.

Wang, Xujie, et al. "Effects of aluminum chloride impregnating pretreatment on physical and mechanical properties of heat-treated poplar wood under mild temperature." *Forests* 13.8 (2022): 1170.

Widyorini, Ragil, et al. "Bonding strength of plywood bonded using phenol formaldehyde mixed with wood bark powder nanofiller." *Journal of the Indian Academy of Wood Science* 17 (2020): 21-33.

Wimmer, R., et al. "Longitudinal hardness and Young's modulus of spruce tracheid secondary walls using nanoindentation technique." *Wood Science and Technology* 31.2 (1997): 131-141.

Xie, Yanjun, et al. "Effects of chemical modification on the mechanical properties of wood." *Eur. J. Wood Prod* 71.4 (2013): 401-416.

Yang, Tiantian, Jinzhen Cao, and Erni Ma. "How does delignification influence the furfurylation of wood?" *Industrial Crops and Products* 135 (2019): 91-98.

Younas, Muhammad, et al. "A review on versatile applications of blends and composites of CNC with natural and synthetic polymers with mathematical modeling." *International journal of biological macromolecules.”* 124 (2019): 591-626.

Zhang, Liangliang, et al. "Thermal behavior and flame retardancy of poplar wood impregnated with furfuryl alcohol catalyzed by boron/phosphorus compound system." *Industrial Crops and Products* 176 (2022): 114361.

Zhang, Zhen, et al. "Grafting polymers from cellulose nanocrystals via surface-initiated atom transfer radical polymerization." *Journal of Applied Polymer Science* 138.48 (2021): 51458.

Zhu, Mingwei, et al. "Highly anisotropic, highly transparent wood composites." *Advanced materials* 28.26 (2016): 5181-5187.